

<https://doi.org/10.1038/s42003-025-08333-z>

Multi-omics analysis of canine aging markers and evaluation of stem cell intervention

Check for updates

Balun Li^{1,3}, Yanheng Ding^{2,3}, Miao Han¹, Zengyu Zhang¹, Zixi Ling¹, Wenlong Zhu¹, Xianjun Zhao¹, Yihua Zhang¹, Changrong Lv¹, Na Li¹, Mingzhi Liao^{2,4}✉ & Jinlian Hua^{1,4}✉

Dogs serve as ideal research subjects for aging studies. In this study, 9 aging-related cell populations are identified through single-cell RNA sequencing of dogs of different ages. Additionally, 9 CD8⁺ T cell senescence-specific markers conserved across species are identified. Furthermore, multi-omics technology is employed to characterize 17 transcriptional and protein markers, along with 5 metabolic markers, associated with stem cell aging. Penitrem A and UDP-N-acetylglucosamine are further validated as two consistent metabolic markers of both individual and cellular senescence. A customized metabolic assessment system and blood-based assessment framework specifically for aging dogs are developed. Notably, it is demonstrated that mesenchymal stem cells, particularly those overexpressing NMNAT1, can delay or reverse aging in dogs. This study sheds light on the mysteries of aging from multiple perspectives and provides a broad target for future research efforts aimed at uncovering the complexity of this fundamental biological process.

In recent years, aging mechanisms and intervention strategies have become the focus of biomedical research¹. In 2023, 12 markers of aging were proposed, including genomic instability, telomere depletion, epigenetic alterations, loss of proteostasis, impaired macroautophagy, dysregulated nutrient sensing, mitochondrial dysfunction, cellular senescence, stem cell depletion, altered intercellular communication, chronic inflammation, and ecological dysregulation¹. From the cellular to the individual, multiple studies targeting different levels of aging are conducted². Many new aging targets and biomarkers have been proposed. However, they remain insufficient.

Dogs are animals closely associated with the development of human society and have been proposed as models for aging research with high translational potential³. Unlike laboratory-dwelling model animals, dogs share many important characteristics with humans, including the same living environment, risk of disease, the calculable aging process, and comprehensive healthcare^{4,5}. However, canine lifespans are much shorter than humans, providing a unique opportunity to recognize the drivers of aging and anti-aging effects³. In 2016, the Dog Aging Project (DAP) was proposed and was undertaken to bring dogs to the attention of aging researchers³. In 2020, Wang et al. created a shared human-canine epigenetic clock model of aging⁶. A growing body of aging research on canine-human commonalities has fueled the burgeoning field of aging⁷.

Cellular senescence and stem cell depletion are well-recognized factors of aging. Cdkn2a (p16) was the first identified marker of cellular senescence and has received widespread attention⁸. With increasing studies, the specificity of p16 in senescence has been questioned, as some p16-overexpressing cells are not senescent e.g., macrophages⁹, mesenchymal stem cells¹⁰, whereas some senescent cells do not express p16^{3,11,12}. Thus, senescence shows different tendencies in different organs and cell types. With the advancement of technology, single-cell genomics and spatial genomics analysis have gradually become the main tools for studying the heterogeneity of aging. Single-cell histology provides reliable evidence for studying heterogeneous senescence by capturing changes in individual cells and thus identifying changes in senescence within a single cell taxon. In addition, multiple senescence markers have been proposed to complement the causation and characterization of senescence (e.g., the cell cycle regulator Cdkn1a (p21), histone H2AX phosphorylation (γH2AX), Lamin B1, matrix metalloproteinase 3 (MMP3), and Lysine Acetyltransferase 7 (KAT7), eIF4E-binding protein 1 (4EBP1)¹³), providing several targets for studying heterogeneous senescence, heterogeneous senescence¹⁴.

Currently, most aging interventions are still in their early stages, and more evidence is needed to support their reversal of aging. Nicotinamide mononucleotide (NMN) (a precursor of NAD⁺) has been shown to have an interventional effect on aging at multiple levels, but most experiments

¹College of Veterinary Medicine, Shaanxi Centre of Stem Cells Engineering & Technology, Northwest A&F University, Yangling, China. ²College of Life Sciences, Northwest A&F University, Yangling, China. ³These authors contributed equally: Balun Li, Yanheng Ding. ⁴These authors jointly supervised this work: Mingzhi Liao, Jinlian Hua. ✉e-mail: liaomz@nwsuaf.edu.cn; jinlianhua@nwsuaf.edu.cn

have been conducted in cells and model animals^{15–17}. Nicotinamide nucleotidyl adenosine transferase 1 (NMNAT1) is a key NAD⁺ biosynthetic enzyme that catalyzes the formation of NMNS into NAD⁺, predominantly located in the nucleus^{18,19}. Studies have shown that supplementation with NAD⁺ precursors such as NMNAT1 has anti-aging benefits^{16,17}. In MSCs, NMNAT1 expression was inversely correlated with known cellular senescence hallmarks such as TP53, CDKN1A, and CDKN2A²⁰. In addition, stem cells therapy is a potential anti-aging strategy²¹. However, in vitro and in vivo senescence of stem cells reduces the regenerative potential and therapeutic efficacy of stem cells^{22–26}. Previous studies have shown that donor senescence leads to altered multilineage differentiation and impaired immunosuppression of MSCs, and replicative passaging results in reduced stemness of MSCs²⁷. Targeting current treatments for complex diseases (including diabetes, liver disease, and aging) through stem cell quality control and genetically modified Mesenchymal stem cell (MSCs) and re-proving their effectiveness is necessary^{28,29}. More evidence is urgently needed to underpin and expand theories of aging and anti-aging programs.

This study collected blood samples and MSCs from Beagle dogs aged 3, 6, and 12 years. Single-cell RNA sequencing (scRNA-seq) of blood Peripheral blood mononuclear cells (PBMCs), and serum metabolomics techniques were used to establish a blood aging atlas in dogs, revealing nine blood cell types associated with aging. Cross-species analysis identified 4 senescence-associated cell types shared between humans and dogs, with CD8⁺ T cells containing 9 senescence markers. Combining multi-omics techniques, 17 transcriptional/protein and 5 metabolic aging markers were identified in MSCs. Two metabolic markers were found to be related to aging. Interventions with MSCs and NMNAT1 overexpression improved liver and kidney function as well as immune status in aging dogs, restoring UDP-N-acetylglucosamine levels, and NMNAT1 regulated Penitrem A levels. Cellular communication analysis showed that aging was accompanied by decreased communication levels, with neutrophil differentiation leading to abnormal immune activation, which accelerated aging. Our research confirms the unveiling of canine aging maps and metabolic changes at the single-cell level, discovering shared aging features between humans and dogs. CD8⁺ T cells are identified as aging markers, with a connection to mitochondrial stability. Furthermore, the efficacy of stem cells and NMNAT1 in modulating the aging process has been validated, shedding light on their pivotal metabolic functions.

Results

Single-cell sequencing identifies cellular population changes in aging dogs

PBMCs were collected from Beagle dogs aged 3, 6, and 12 years for scRNA-seq analysis, alongside serum samples for metabolomic analysis (Fig. 1a). scRNA-seq data from 17,575 cells were processed using the Seurat³⁰ pipeline, where batch effects among the samples were identified and subsequently corrected using the Harmony³¹ algorithm (Supplementary Fig. 1a). Leiden³² clustering algorithm categorized these 17,575 cells into 31 distinct clusters (Supplementary Fig. 1b).

Using known cell type markers, the 31 clusters were further grouped and annotated into nine major cell types (Fig. 1c and Supplementary Fig. 1e), including CD8⁺ T cells/NK cells, CD4⁺ T cells, neutrophils, B cells, plasma cells, polymorphonuclear myeloid-derived suppressor cells (PMN-MDSCs), platelets (Supplementary Fig. 1c, d), eosinophils/basophils and monocytes/DCs. These major cell types were further annotated at a more granular level using additional markers (Supplementary Fig. 2).

Plot1cell³³ was utilized to visualize these annotated cells, displaying the UMAP embedding of the cells and the distribution of each cell type across different ages (Fig. 1b). The abundance of each cell type showed distinct changes throughout the aging process (Fig. 1d). The number of CD4⁺ T cells in dogs gradually decreases with age, with a particularly significant decline observed in middle-aged and elderly stages (Fig. 1e). The total number of eosinophils/basophils shows a linear decline with age, while myeloid-derived suppressor cells exhibit a linear increase (Fig. 1e).

Neutrophils, which represented the largest proportion of cells in all samples (Fig. 1d), were subdivided into 21 clusters using the Leiden clustering algorithm (Supplementary Fig. 3a). Monocle3³⁴ was utilized to construct the cell trajectory of neutrophils (Supplementary Fig. 3b, c), and cell potencies predicted by CytoTRACE2³⁵ were used to determine the starting point of this trajectory. Additionally, Ucell³⁶ was employed to score all neutrophils based on KEGG pathways. Notably, Cluster 6 exhibits the lowest grade of differentiation (Supplementary Fig. 3d), depressed glycolysis gluconeogenesis, and activated ribosome metabolism (Supplementary Fig. 3e), suggesting that Cluster 6 represents immature neutrophils³⁷.

Identification of aging-related cell types and common aging biomarkers across species

To investigate the changes in different cell types during the aging process in dogs, this study calculated the Pearson correlation coefficients (PCC) for all age groups across all cell types (Fig. 2a). Subsequently, a pairwise Pearson correlation coefficient (PCC) comparison was used to screen the potential age-related celltypes (Fig. 2b). Total nine cell types were identified as age-changed cell types, including neutrophil, immature neutrophil, CD4-monocyte, myeloid cDC2, basophil, CD4⁺ effector memory T cell (CD4⁺ TEM), CD8⁺ effector T cell, CD8⁺ memory T cell and plasma cell. UMAP embedding for these types of cells also shows heterogeneity among different ages (Fig. 2c).

Furthermore, a monitoring system for the cytological assessment of aging in dogs was proposed and its potential for cross-species application was evaluated. In this system, the consistency between human aging and dog aging was tested. By comparing aging biomarkers in corresponding human cell types³⁸, four cell types were identified where both humans and dogs exhibited significant and consistent directional changes in these biomarkers (Supplementary Fig. 4a, b). Specifically, the study tested the consistent markers previously mentioned in CD8⁺ T cells, which can represent the cross-species aging process (Fig. 2d and Supplementary Fig. 4c). Further characterization of these ten blood markers predicted by scRNA-seq was conducted by comparing the blood q-PCR data of young and aging dogs. The results indicated that nine of these markers were consistent with the predicted trends (Fig. 2e).

Alterations in cellular communication during aging

In-depth studies of cell communication have shown that cell-cell interactions and signaling undergo significant changes during life, which are closely related to aging. Further investigation into cell communication reveals that the MDSC cellular potency score predicted by cytoTRACE2 undergoes significant alterations with age (Fig. 3a), this reveals the complexity of age-related changes in the function of MDSCs in the immune system. Simultaneously, other immune cells also exhibit significant changes in gene expression levels during aging, further emphasizing the dynamic adjustment of the immune system during aging (Fig. 3a).

Given the immunosuppressive effects of MDSCs on these immune cells, CellChat³⁹ was employed to conduct a cell communication analysis based on data pertaining to Secreted Signaling, ECM-Receptor interactions, Cell-Cell Contact, and Non-protein Signaling. The results indicate that the number of cell-cell communication decreases with age (Fig. 3b). We were surprised to find that cell communication intensity was enhanced in the middle-aged and old-aged range, but significantly decreased at the end of senescence (Fig. 3c). This finding suggests that there may be a complex Dynamic equilibrium process rather than a monotonic decrease in cell communication.

Further analysis revealed that cell communication in young adults performs better in maintaining cell proliferation and immunomodulation, and that young adults are better at maintaining cell proliferation and immunomodulation than young adults, the genes involved include Transforming growth factor beta (TGF- β), Fas ligand (FASLG) and platelet endothelial cell adhesion molecule-2 (PECAM2), among others (Fig. 3d). In contrast, cell communication in the elderly is more focused on apoptosis and the inflammatory response, involving genes such as Bcl-2-related

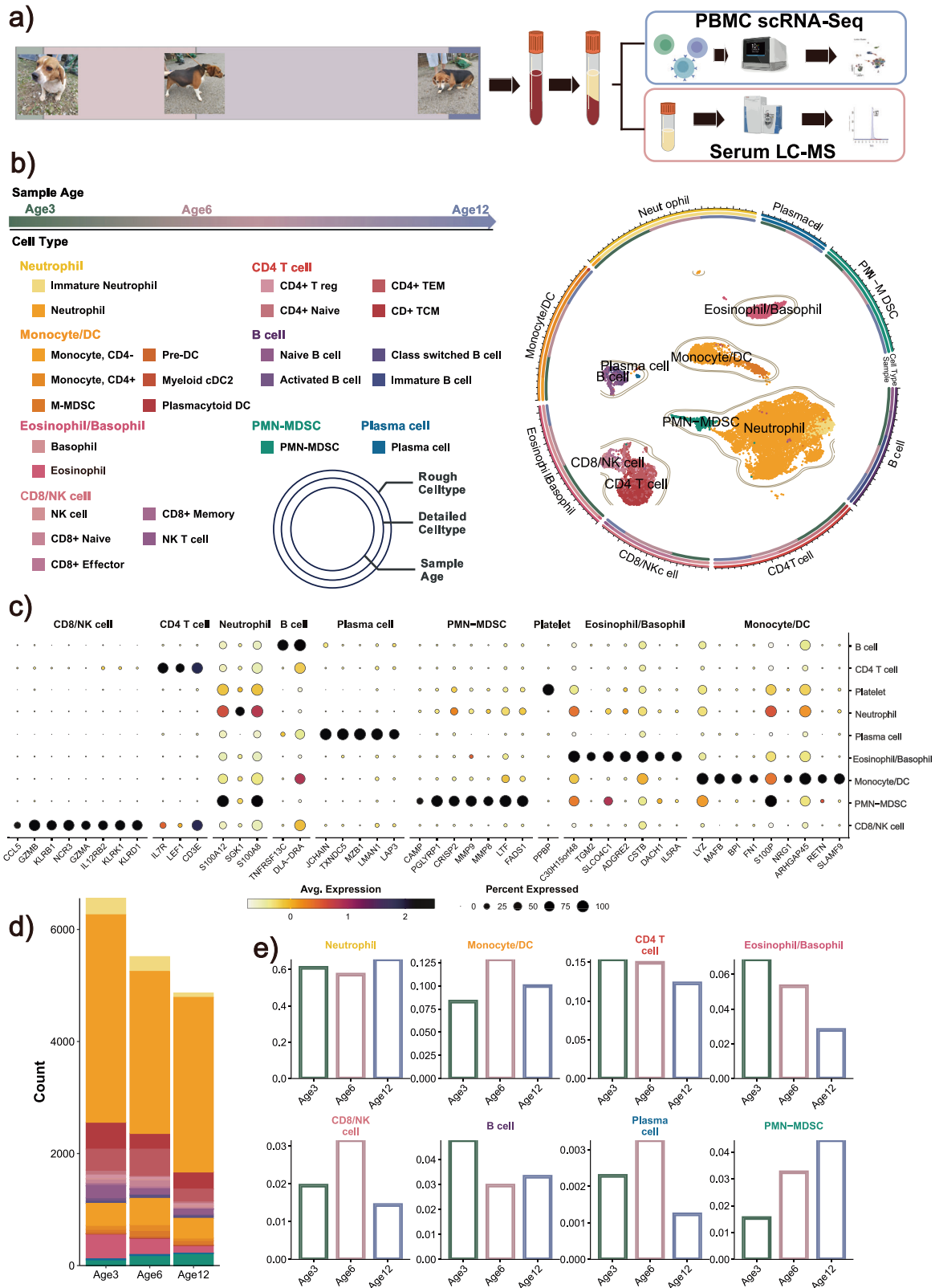


Fig. 1 | scRNA-seq sequencing during aging in dogs. a Schematic of this study. scRNA-seq of PBMC and LC-MS of serum were conducted on Beagles at the ages of 3, 6, and 12 years, respectively. Photos of the dogs were taken from the subjects and photographed by the authors. **b** Classification of cell subpopulations in scRNA-seq.

c The expression of cell type marker genes among cell types. **d** The number of each type of cell in different samples. **e** The proportion of each type of cell in different samples.

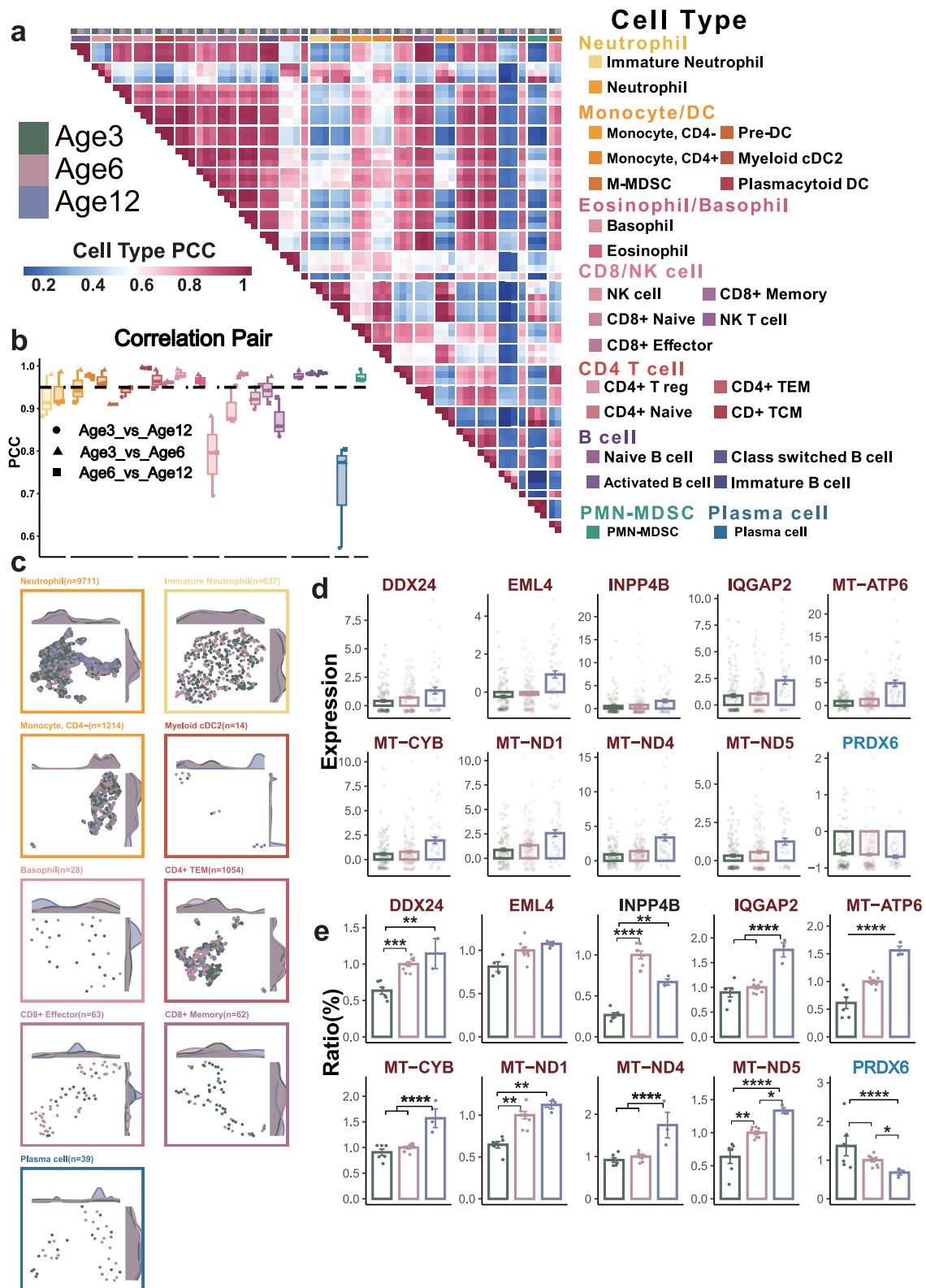


Fig. 2 | Identification of aging-related cell types and common markers of aging across species. **a** The Pearson correlation between different cell types across different samples. **b** The Pearson correlation of the same cell type across various samples, while the dashed line indicates a threshold of 0.95. **c** The distribution of the nine age-associated cell types across different samples. **d** The expression of reported genes that

demonstrate age-related upregulation (red) or downregulation (blue) in CD8T cells. **e** qPCR validation of age-related up-regulated (red), down-regulated (blue), and invalid (black) genes in CD8T cells. Values in E are mean \pm SD; $n = 3$ biologically independent samples per group; ns > 0.05, * $p < 0.05$, ** $p < 0.01$, *** $p < 0.001$, **** $p < 0.0001$ determined by repeated measures of ANOVA.

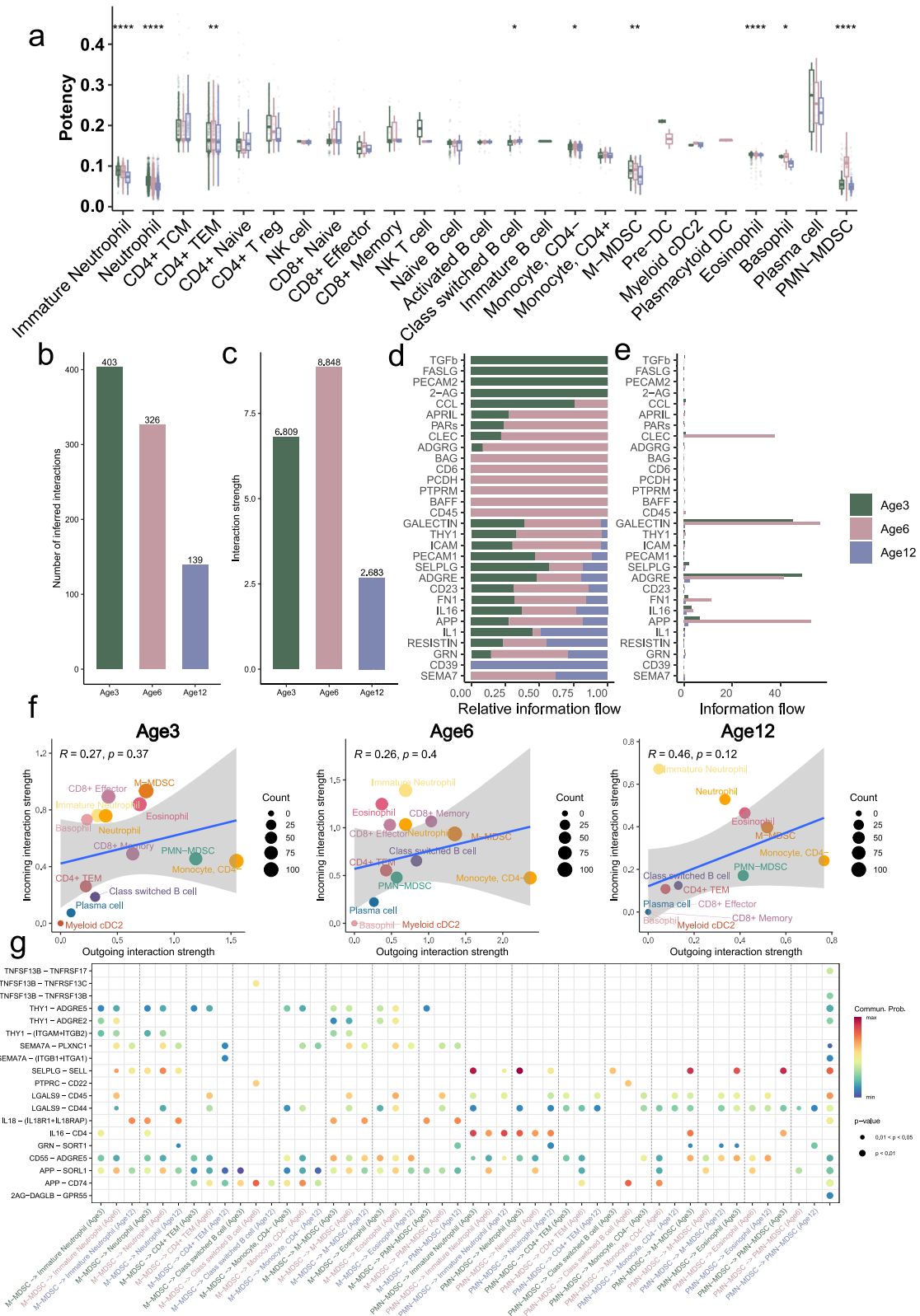


Fig. 3 | Alterations in cellular communication during aging. a Predicted cell potency, where different color represent different ages. Asterisks indicate a significant difference across ages tested by Wilcoxon rank-sum test. The levels of significance are denoted as follows: * $p < 0.05$, ** $p < 0.01$, *** $p < 0.001$, **** $p < 0.0001$. **b** Number of cellular communications across different ages. **c** Strength of cellular communication

across difference ages. **d** Relative information flow for different samples. **e** Information flow for different samples. **f** Scatter plot showing the income strength and outgoing strength for each cell type in samples of different ages. **g** Communication probability of regulation of ligand receptor pairs from MDSCs to other immune cells.

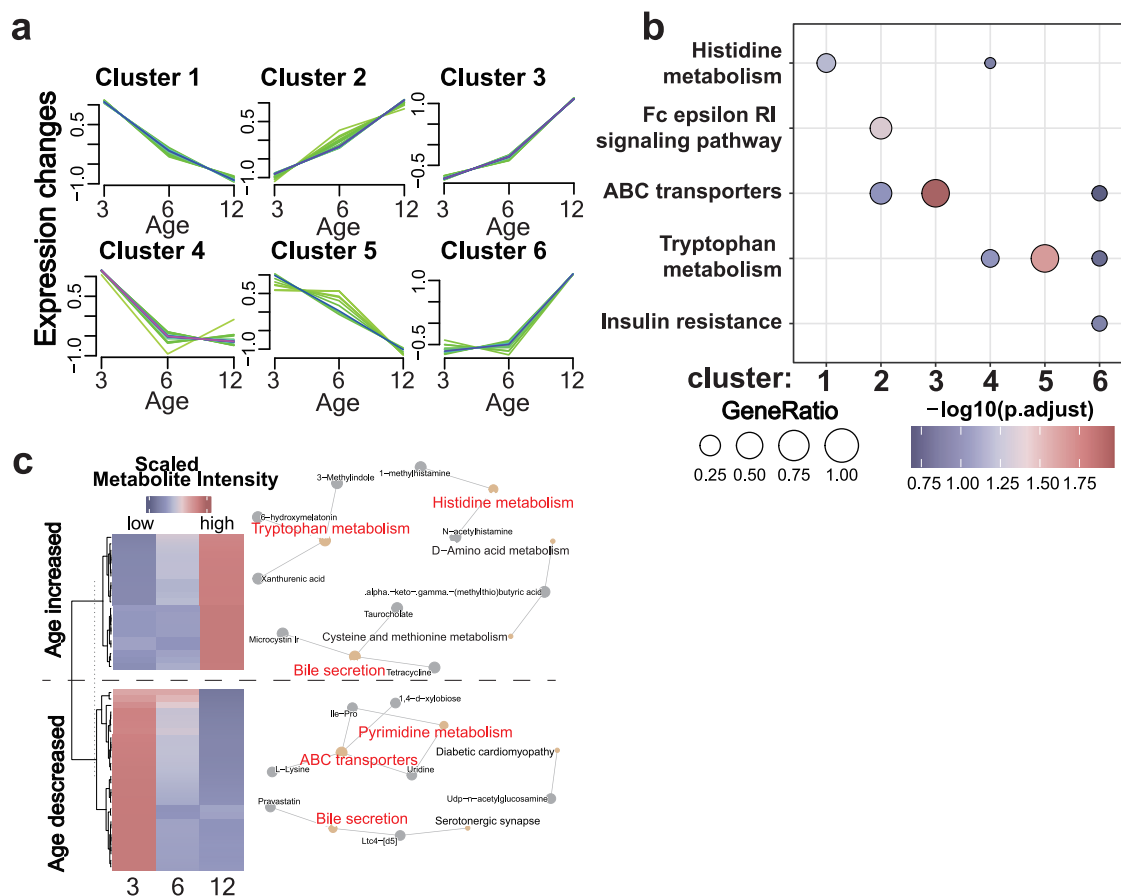


Fig. 4 | Serum metabolome analysis reveals metabolic features of canine aging. a 51 age-associated metabolites were identified, and these metabolites were grouped into six clusters with different patterns. b The results of the KEGG enrichment

analysis for these six clusters. c The intensity of age-increased and age-decreased metabolites, along with their KEGG enrichment, was displayed.

anti-apoptotic gene (BAG), CD6, pro-cadherin (PCDH) and CD45 (Fig. 3d). These differences suggest that the focus of cellular communication may shift with age, from promoting growth and immune homeostasis to responding to injury and inflammation.

Notably, the increase in glucose metabolism, as well as the incorporation of glucose metabolism-related communications, such as CLEC and GALECTIN family members, were predicted to be important markers of rapid progression of aging in middle-aged and older adults (Fig. 3e). This finding highlights the critical role of glucose metabolism in the aging process and its intimate connection with cellular communication. In addition, we also observed that immature neutrophil communication was enhanced with the development of aging (Fig. 3f), which is consistent with our previous findings that aging affects the differentiation rate of neutrophil, suggesting that aging may play an important role in the aging process, this, in turn, leads to a reduction in its immunosuppressive capacity (Supplementary Fig. 3). The findings lend further support to the hypothesis that the immune system declines with age and suggest that our immature neutrophil may play a role.

Serum metabolome analysis reveals metabolic features of canine aging

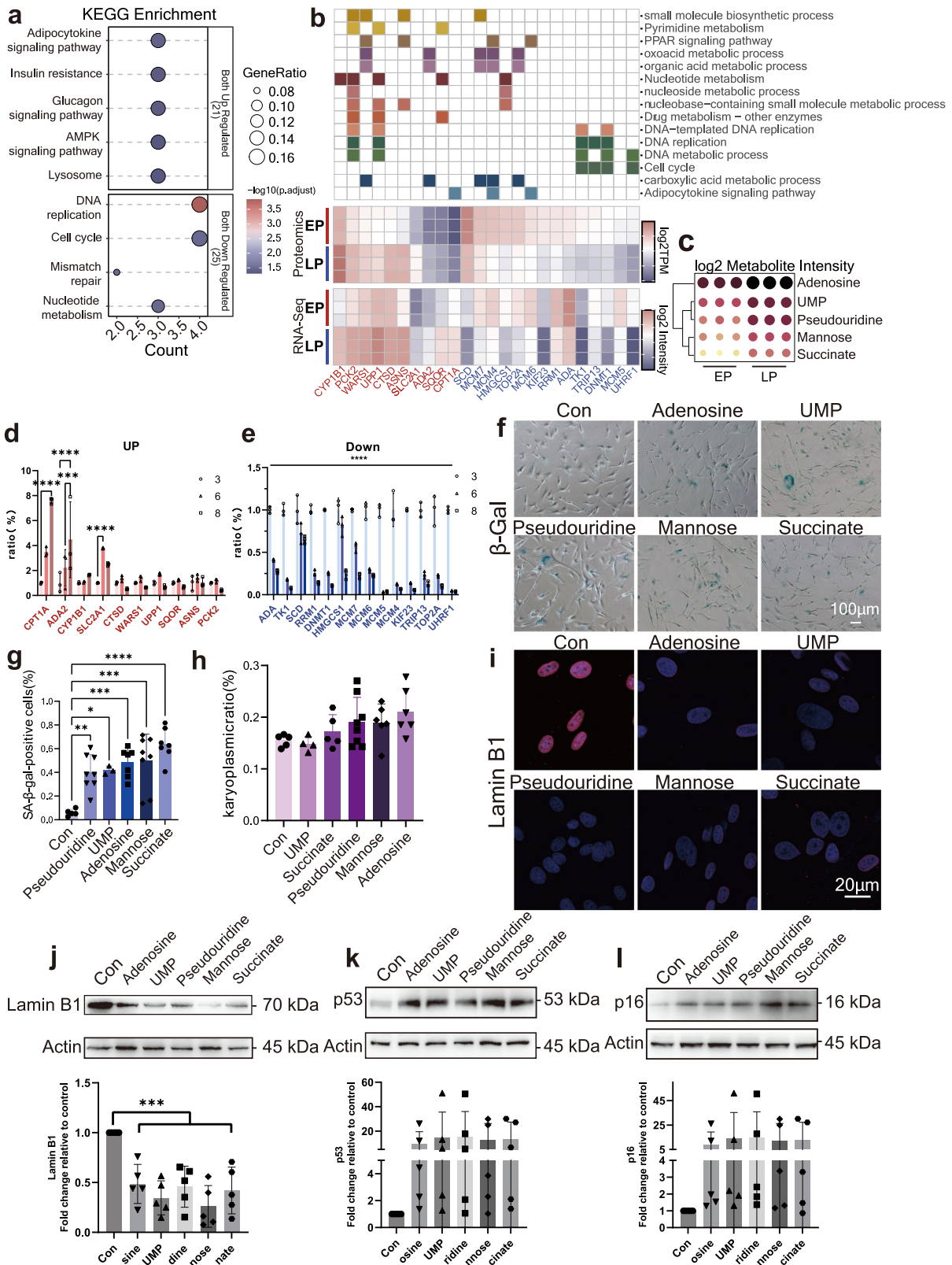
To explore the dynamic changes in serum metabolites during dog aging, correlation tests were employed to calculate the Spearman correlation coefficient for each metabolite in relation to age, resulting in a total of 51 age-associated metabolites ($p < 0.05$). Subsequently, metabolites were clustered into 6 clusters (Fig. 4a) using the fuzzy C-means clustering algorithm, with clusters 1, 4, and 5 representing those that decreased with age, and clusters 2, 3, and 6 representing those that increased with age. Enrichment analysis of these metabolites suggests that ATP synthase binding cassette

transporters (ABC transporters) and insulin resistance are key markers of aging (Fig. 4b, c). Additionally, pyrimidine metabolism shows a gradual increase with age, while sterol metabolism gradually decreases (Fig. 4c).

Confirmation of cellular senescence mechanisms using a continuous passage stem cell model

A cellular senescence model for MSCs subjected to multiple passages was established. An integrated multi-omics analysis, encompassing transcriptomics, proteomics, and metabolomics, was then conducted to gain insights into the aging process. Gene Set Enrichment Analysis (GSEA) utilizing aging-related metabolites from the Aging Atlas⁴⁰ dataset validated the senescence model (Supplementary Fig. 5a). This finding provides a theoretical basis for the observed slowed proliferation and heightened nutritional requirements of high-passage MSCs during culture.

A series of screening methods were employed to identify potential multi-level biomarkers during the MSCs aging process. Firstly, genes that underwent significant changes at both the transcriptional and protein levels during aging were retained. Enrichment analysis of these genes revealed that glucose metabolism levels increased while DNA replication levels decreased during MSC aging (Fig. 5a and Supplementary Fig. 5b), providing a theoretical explanation for the slowed proliferation and increased nutritional demands of high-passage MSCs during culture. Subsequently, enrichment analysis of the metabolites that showed significant changes in both the Aging Atlas data and our experimental data revealed a strong correlation with pyrimidine metabolism (Supplementary Fig. 5c). Following this, genes and metabolites with intersections in metabolic pathways were identified as potential MSC aging-related biomarkers. This process led to the



identification of 24 gene/protein biomarkers (Fig. 5b) and 5 metabolic biomarkers (Fig. 5c).

Quantitative Real-Time PCR (QRT-PCR) identification of multiple generations of MSCs showed that 3 of the 10 enriched genes significantly upregulated with senescence were stably upregulated during senescence (carnitine palmitoyltransferase 1A (CPT1A), Adenosine deaminase 2

(ADA2), cytochrome P450 family 1 subfamily B member 1 (CYP1B1)) (Fig. 5d). All the enriched genes that decreased significantly with senescence were negatively correlated with senescence (Fig. 5e). All primers involved are listed in Supplementary data 1.

Adding the enriched 5 senescence-associated metabolites to the culture environment of MSCs promoted the β-Galactosidase’s activity of MSCs

Fig. 5 | Identification of senescence markers of canine stem cells by multiple omics. **a** The results of the KEGG enrichment analysis for the intersection of differentially expressed genes (DEG) and differentially expressed proteins (DEP). **b** The expression profiles of the screened markers at the transcription and translation levels, as well as the pathways involving the corresponding markers. **c** The Intensity of screened marker metabolites. **d** qPCR was performed at the mRNA level to identify the markers up-regulated with senescence in the multigenerational MSCs. **e** qPCR was performed at the mRNA level to identify the markers down-regulated with senescence in the multigenerational MSCs. **f** β -galactosidase staining of MSCs

treated with five senescence promoters. **g** Analysis of β -Galactosidase Positivity Rate in MSC. **h** Nuclear-to-cytoplasmic ratio analysis of MSCs treated with five senescence promoters. **i** Lamin B1 immunofluorescence staining of MSCs treated with five senescence promoters. Representative images and Densitometry of Western blot analysis of Lamin B1 (**j**), p53 (**k**) and p16 (**l**) in total proteins extracted by metabolite-treated MSCs ($n = 5$ biological replicates groups). Scale bar for **f** is 100 μ m. Scale bar for **i** is 20 μ m. Values in **d**, **e**, **b**, **h**, **j**, **k**, **l** are mean \pm SD; $n = 5$ per group; * $p < 0.05$, ** $p < 0.01$, *** $p < 0.001$, **** $p < 0.0001$ determined by repeated measures of ANOVA.

(Fig. 5f, g). The nucleo-cytoplasmic ratio reflects organelle redundancy and is an indicator of cellular senescence, and Giemsa staining showed that the addition of five metabolites expanded the nucleo-cytoplasmic ratio of MSCs (Fig. 5h, Supplementary Fig. 5d). Lamin B1 staining also confirmed the senescence-promoting effects of all senescence-related metabolites (Fig. 5i). Western blot assays on senescence-associated metabolite-treated MSCs revealed that all five metabolites decreased Lamin B1 expression (Fig. 5j) of MSCs and elevated the levels of senescence-associated p53 (Fig. 5k) and p16 (Fig. 5l) protein expression.

Integrated analysis of systemic and cellular metabolomes uncovers common metabolic hallmarks of aging

To delve into the concurrent alterations occurring at both cellular and individual levels during the aging process in dogs, a comparative analysis was undertaken between the metabolites that underwent notable variations in MSCs and those that exhibited significant changes in serum. This analysis identified two metabolites—Penitrem A and UDP-N-acetylglucosamine—that significantly increased with aging in both MSCs and serum (Fig. 6a).

Giemsa staining showed that Penitrem A and UDP-N-acetylglucosamine led to cell enlargement and morphological swelling, consistent with a trend of aging changes (Fig. 6d, Supplementary Fig. 6e). Both molecules enhanced CASPASE3 expression and reduced mitochondrial membrane potential levels, showing the promoting effect of both on aging (Supplementary Fig. 6a–d). β -galactosidases staining confirmed the senescence association of Penitrem A and UDP-N-acetylglucosamine (Fig. 6b, c). Lamin B1 is a member of the nucleofibrin family, whose main function is to maintain the integrity of the cytoskeleton and participate in cell proliferation and senescence by affecting chromosome distribution, gene expression, and DNA damage repair. Lamin B1 staining confirmed the effect of Penitrem A and UDP-N-acetylglucosamine on the integrity of the cytoskeleton in the aging phase (Fig. 6e). Protein and RNA levels confirmed that Penitrem A and UDP-N-acetylglucosamine increased the expression levels of p53, p16, and Lamin B1, further confirming the effect of crude senescence (Fig. 6f–i). Furthermore, we analyzed the changes in Penitrem A and UDP-N-acetylglucosamine in aging by mass spectrometry to support metabolic changes during aging (Supplementary Fig. 6f). In summary, we have identified and validated common metabolic markers of aging at both cellular and individual levels: Penitrem A and UDP-N-acetylglucosamine. The discovery of these markers provides targets for the assessment and intervention of aging.

MSCs loaded with NMNAT1 reduce the degree of canine aging

A total of 19 police dogs were enrolled in our study to examine the effects of aging. To ascertain the patterns of blood index alterations during aging, a comprehensive analysis of blood routine and biochemical parameters was conducted on canines aged 3, 6, 8, 10, and 12 years (Supplementary Fig. 7). Blood routine data showed changes in immune cells and hematopoiesis. Our results showed that eight blood routine data increased with age, including significantly increased neutrophil counts, white blood cells, and number of monocytes (Supplementary Fig. 7a). Changes in immune cells during senescence were consistent with trends in response to our single-cell transcriptomic data (Fig. 1e and Supplementary Fig. 2h).

Our data showed that phosphorus ions and Alkaline phosphatase increased gradually with age (Supplementary Fig. 7c). Six biochemical

indexes decreased with age, among which calcium ion decreased significantly, which was closely associated with the calcium loss that occurred gradually during aging (Supplementary Fig. 7d). In addition, data on a gradual decline in blood biochemistry reflect an overall decline in hepatic and renal function, with decreases in creatinine and urea nitrogen levels showing a decline in renal function, whereas cholesterol, the gradual decrease of lipase and total protein (TP) contents was related to the decline of liver function in aging (Supplementary Fig. 7d).

Subsequently, 12 of the dogs were administered with anti-aging therapeutic interventions. MSCs were engineered to overexpress NMNAT1, and their expression levels were subsequently validated via Western blot analysis (Supplementary Fig. 7e). An examination of blood routine and biochemical data across three distinct groups was undertaken, with a focus on evaluating alterations in senescence-associated biomarkers (Fig. 7a, b). MSCs intervention reduced White Blood Cell counts (WBC), lymphocyte (LYM), and neutrophil levels (NEU#) in senescence and increased the number and proportion of Basophil granulocyte within one month, whereas NMNAT1 prolonged the anti-aging effect (Fig. 7a). In the process of aging, the requirement of bone marrow hematopoiesis is increased and metabolism is strengthened. Mean platelet volume (MPV), which reflects bone marrow hematopoietic function and platelet status, showed an upward trend in aging (Supplementary Fig. 7a). MSCs treatment reduced MPV levels in response to the restoration of blood metabolism, and the addition of NMNAT1 similarly enhanced this effect of MSCs (Fig. 7a). A decrease in TP in senescence was found in our study, whereas intervention with MSCs and NMNAT1 elevated TP levels, portending a restoration of liver function (Fig. 7b).

To evaluate the effectiveness of stem cell therapy in aging dogs at the metabolic level, we developed a scoring system based on metabolites that showed significant changes during natural aging in dogs (Fig. 7c). Gene set variation analysis (GSVA) was applied to score the samples before and after stem cell therapy. The results showed that, at the metabolic level, treatment MSCs can effectively slow down the aging process, while treatment with NMNAT1- MSCs can partially reverse it.

A deeper exploration into the alterations of individual metabolites during stem cell therapy aimed at mitigating aging effects was undertaken. Our attention was centered on metabolites displaying prominent alterations during the natural aging process in dogs, which were subsequently grouped into eight distinct categories based on their characteristic expression patterns. (Fig. 7d). Enrichment analysis showed that, consistent with our previous data, senescence was accompanied by a decrease in histone metabolism, tryptophan metabolism, bile acid metabolism, cholesterol metabolism, and taurine metabolism (Fig. 4b, c). Our previous analysis showed that senescence was accompanied by an increase in glucose metabolism and a decrease in DNA replication as well as histone metabolism (Fig. 5a). Here, changes in individual metabolites are highly consistent with changes in cell metabolism. The FC Epsilon Ri signaling pathway is up-regulated in senescence, which is involved in antigen presentation mediated by IgE and exhibits aberrant immune activation in senescence. Niacin decreases in aging, and treatment with MSCs increases niacin levels in individuals, demonstrating that MSCs themselves have a role in complementing and restoring niacin levels, while nmnat1-MSCs also have a restorative role. Our previous results revealed that Penitrem A and

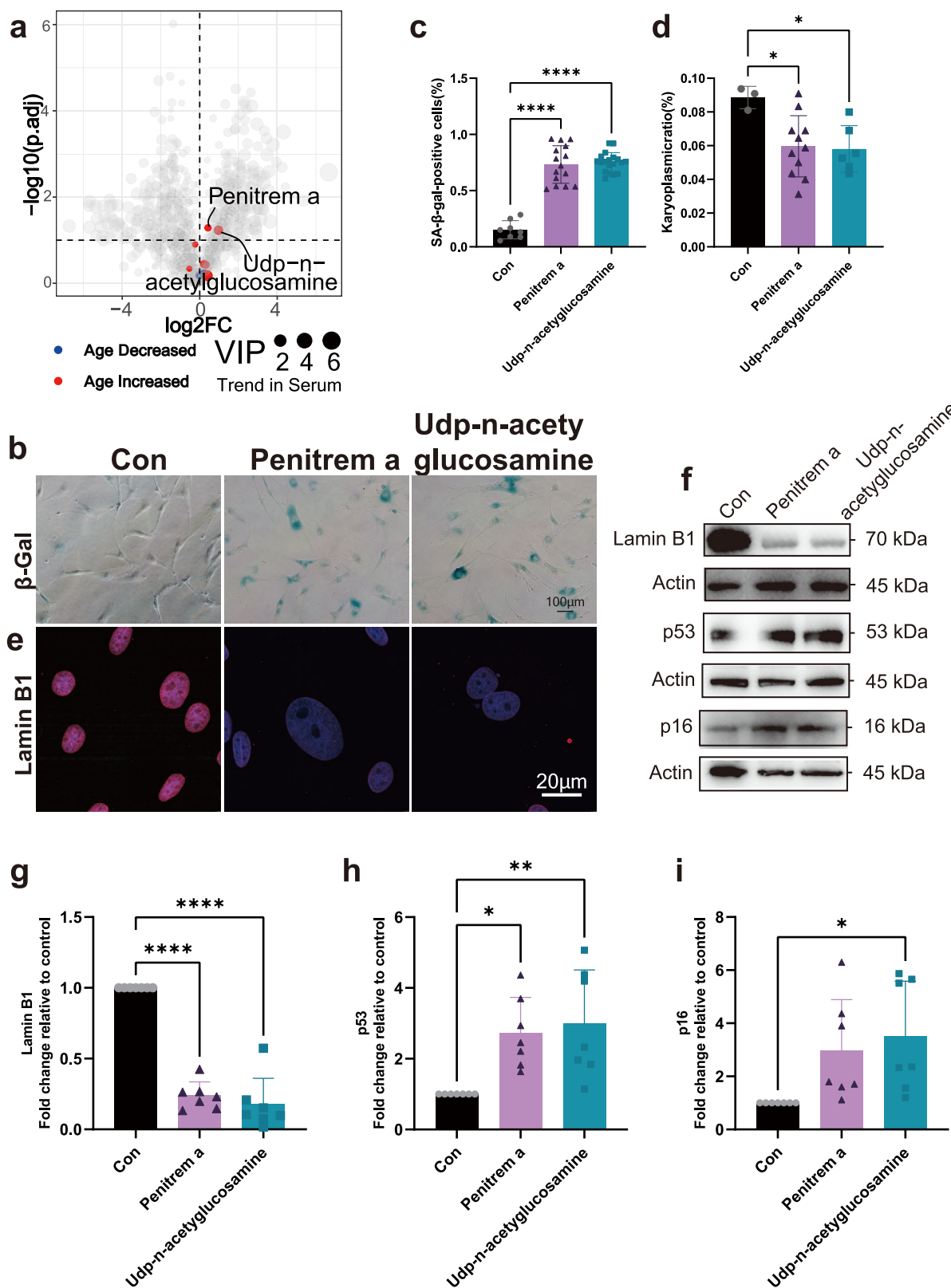
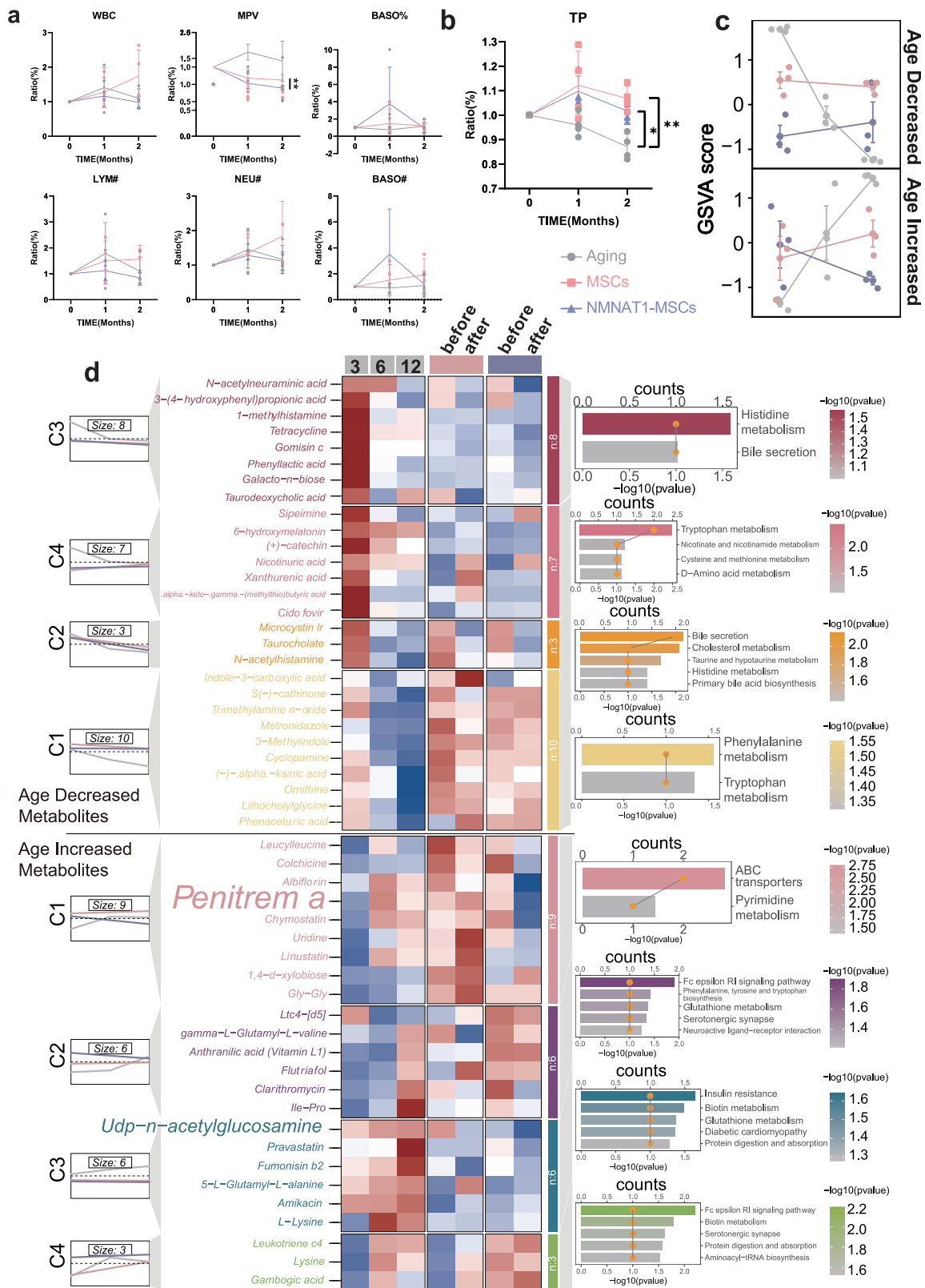


Fig. 6 | Integrated analysis of systemic and cellular metabolomes uncovers common metabolic hallmarks of aging. **a** The volcano plot illustrates the differential metabolites in the aging process with MSCs. Here, the color of each dot represents the trend of the corresponding metabolite concentrations in the serum over time. **b** β -galactosidase staining of MSCs after Penitrem A and udp-n-acetylglucosamine treatment. **c** Analysis of β -Galactosidase Positivity Rate in MSC. **d** Nuclear-to-cytoplasmic ratio analysis of MSCs after Penitrem A and udp-n-

acetylglucosamine treatment. **e** Lamin B1 immunofluorescence staining of MSCs after Penitrem A and udp-n-acetylglucosamine treatment. **f** Representative images and Densitometry of Western blot analysis of Lamin B1 (**g**), p53 (**h**) and p16 (**i**) in total proteins extracted by metabolite-treated MSCs ($n = 7$ biological replicates groups) Values in **d**, **e**, **h–i** are mean \pm SD; Scale bar for **b** is 100 μ m. Scale bar for **e** is 20 μ m Values in **d**, **e**, $n = 3$ per group; Values in **g–i**, $n = 7$ per group; *** $p < 0.001$, **** $p < 0.0001$ determined by repeated measures of ANOVA.



UDP-N-acetylglucosamine induced senescence at the individual and stem cell levels (Fig. 6). Interestingly, our investigation revealed that the anti-aging treatment involving MSCs led to a marked decrease in UDP-N-acetylglucosamine levels, and this effect was further augmented by the notable enhancement observed with NMNAT1. This is the first report that MSCs reverse senescence by reducing UDP-N-acetylglucosamine

expression. Furthermore, NMNAT1 significantly reduced the expression of Penitrem A, implying that the association of NMNAT1 with MSCs had a strong synergistic relationship, and MSCs carrying NMNAT1 showed a strong intervention effect on 2 markers of senescence. Our findings raise optimism about the role of genetically modified MSCs in a variety of diseases and aging.

Fig. 7 | Intervention of stem cells and NMNAT1 in aging dogs. a Effects of MSCs and NMNAT1-loaded MSCs on the recovery of blood routine indexes in aging dogs. WBC: White Blood Cell Count; MPV: Mean platelet volume; BASO%: Percentage of basophils; LYM#: Absolute lymphocyte count; NEU#: Absolute neutrophil count; BASO#: Basophil count absolute. **b** Effects of MSCs and NMNAT1- MSCs on total protein (TP) recovery in aging dogs. **c** GSVA analysis using metabolites that increase with age and decrease with age. The gray line represents the process of natural aging, the red line represents the process of treating aging with MSCs, and the blue line represents the process of treating aging with NMNAT1_MSCs. **d** Expression Changes of Aging-Associated Metabolic Markers in Natural Aging and Before and

After Stem Cell Therapy. Aging-related metabolic markers were divided into 8 groups according to the expression changes that decreased or increased with age during aging. Columns of the heatmap represent: natural aging process, before and after MSCs therapy, and before and after NMNAT1-MSCs therapy. The average expression change trend of each cluster is plotted in the line graph, where gray represents the natural aging process, pink represents the MSCs treatment process, and blue represents the NMNAT1-MSCs treatment process. The KEGG pathways enriched by the metabolites in each cluster are displayed in the bar graph. Values in A, B are mean \pm SD; $n = 4$ per group; * $p < 0.05$, ** $p < 0.01$ determined by repeated measures of ANOVA.

Discussion

Dogs have become an ideal model for studying human aging^{5,6}. Ammons' research has revealed disease similarities between dogs and humans, further confirming that dogs are an ideal model for human disease research⁴¹. In addition, Zeng et al performed blood-based RNA sequencing on old dogs, confirming that canine aging is associated with metabolism and immune function, and treated old dogs with classical anti-aging methods²¹. To further unravel the mysteries of aging, this study systematically reveals the molecular features of aging across species by integrating multi-omics data on canine blood and Mesenchymal stem cell (MSCs), and provides new insights into the mechanisms of aging in dogs, moreover, biomarker-based stem cell intervention strategies have been developed, which provides a new perspective for understanding the mechanism of mammalian aging.

Previous studies have performed detailed single-cell analyses of various immune cell types in dogs, highlighting changes in immunity in disease and making prospective contributions to canine immune cell delineation⁴¹. By constructing a cross-species single-cell senescence signature map, we identified nine age-related immune cell subsets, including neutrophil, CD4-monocytes, and CDC2 dendritic cell. Studies have shown that T cell lineage commitment and differentiation regulated by Tox change in aging²¹. In addition, previous studies have found that B cells and neutrophil decline as dogs age^{41,42}. Similar to humans, dogs maintain long-term immune homeostasis after development into adult individuals, while presenting a rapid decline in function at a specific stage in middle age and old age, mostly 6–8 years in police dogs and 40–60 years in humans. This study further expands the researchers' understanding of immunosenescence. Our results show that changes in T cells in aging are heterogeneous across cell subtypes. The changes in the numbers of most immune cells (T cells, B cells, and NK cells) in aging are similar to the results of cell communication, showing unique changes (severely decreased or increased) in the middle-aged and elderly stages, and the effects of aging on the number of T cells, B cells, and NK cells are similar to those of aging, it is more stable in the young stage and at the end of life. CD4 + Tregs decline in aging, a class of cells that represents an immunosuppressive population, implying that immune deregulation is associated with rapid frailty in middle and old age. For neutrophil, this study found an enrichment of more poorly differentiated neutrophil in aging individuals, consistent with slower cellular self-renewal during aging. Notably, contrast with human aging features revealed 4 evolutionarily conserved aging-associated cell populations, suggesting that mammals may regulate immune system decline through common mechanisms. Further focusing on CD8 + T cells, we screened 9 core senescence markers, such as DDX24, EML4, etc., among them, the enrichment of MT-ATP6, MT-CYB, and five other mitochondrial genes (55.6%) directly confirmed the central position of mitochondrial dysfunction in aging. This finding provides new cellular-level evidence for the theory of cross-species energy metabolism imbalance.

By establishing an in vitro senescence model of MSCs and multi-omics analysis, we identified 17 molecular markers and 5 metabolic markers. Studies have found that abnormal glucose metabolism and decreased DNA replication capacity are key mechanisms driving MSCs aging⁴³. Reduced glucose uptake leads to insufficient energy supply, affecting cell function; at the same time, metabolic wastes such as ROS accumulation exacerbate cell damage^{44,45}. In addition, the decline of DNA replication capacity affects cell

proliferation and genetic information stability, and telomere shortening and weakened DNA damage repair capacity further promote aging^{46,47}. In this study, multi-omics integrated analysis indicated that abnormal glucose metabolism and decreased DNA replication capacity may be the key mechanisms driving stem cell aging. Of particular concern is the progressive elevation of pyrimidine metabolism and the downward trend of sterol metabolism during canine aging, suggesting that ABC transporters may serve as hub molecules for cross-species metabolic reprogramming.

Although clinical anti-aging trials of drugs such as metformin have been conducted, broader evaluation systems need to be developed^{48,49}. In humans, primates, and other animals, evaluations of aging primarily rely on DNA analysis and protein detection of key aging organs, yet these methods also face challenges in rapid clinical application⁴⁹. Blood routine tests and blood biochemical data are readily accessible and technically mature in clinical settings⁴⁹. The combination of these two detection methods can provide comprehensive health information, particularly in the context of aging⁴⁹. Blood routine tests swiftly reveal an individual's hematopoietic capacity and immune function, while blood biochemical data assess liver and kidney functions, blood glucose and lipid levels, and ion concentrations⁴⁹. In this study, a three-level aging assessment system based on blood routine-biochemical-metabolomics was established. Blood parameters showed that neutrophil monocyte counts increased with age, while basophil granulocyte and TP levels increased significantly after stem cell intervention, it is suggested that MSCs may play an anti-aging role by regulating liver synthetic function and immune homeostasis. By incorporating different working dog breeds (e.g., drug-detecting beagles vs. guard Belgian horse dogs), we demonstrate for the first time that differences in workload accelerate changes in specific indicators of aging (e.g., Alkaline phosphatase levels), and we demonstrate that differences in workload can accelerate the development of aging-related traits, this has important reference value for the development of personalized anti-aging programs. MSCs are widely available and easily accessible, making them a good target for research and intervention in aging. The replicative senescence model of MSCs has emerged as a pivotal tool for simulating aging processes and validating aging biomarkers. The in vitro replicative senescence of MSCs efficiently recapitulates the dynamic signaling pathway alterations and molecular shifts observed during aging, enabling rapid screening of aging biomarkers and evaluation of anti-aging interventions through genetic engineering and small-molecule treatments. Notably, MSCs' pluripotent differentiation capacity allows their senescent phenotypes to mirror age-related changes across multiple organs and tissues, transcending the limitations of terminally differentiated cell models. The accessibility of aged MSCs further facilitates multi-omics profiling—integrating transcriptomics, epigenomics, proteomics, and metabolomics—to construct a comprehensive molecular atlas of aging. This multi-layered dataset provides critical support for the discovery and validation of aging biomarkers, bridging the gap between basic aging research and translational applications.

In essence, our research has outlined a comprehensive single-cell atlas of canine-human aging. Furthermore, this study has confirmed molecular markers and metabolic markers of stem cell aging, providing a broad range of indicators for studying the commonalities of aging in individuals and cells. Moreover, the stem cell aging markers provided by this study offer a

comprehensive set of metrics for assessing stem cell quality. This study has established an evaluation system for anti-aging effects, which leverages cost-effective blood routine tests, biochemical tests, and metabolomic analysis to achieve precise evaluations of aging and anti-aging interventions. By applying this evaluation system, we have confirmed the anti-aging effects of MSCs and NMNAT1, as well as their crucial roles in regulating immunity and metabolism. However, it is worth noting that our study still has limitations. Although the existing canine cohort covers four breeds, the individual age distribution (especially the extreme aging group) and gender balance still need to be expanded. In the future, it is necessary to establish a large-scale aging canine cohort across regions and breeds. In addition, the current analysis focuses on blood and MSCs, while the molecular characteristics of key aging organs such as brain and liver have not yet been resolved, and multi-tissue verification needs to be carried out in combination with technologies such as spatial transcriptome. The long-term effects (>12 months) and potential side effects of MSCs treatment need to be followed up longitudinally. In addition, NMNAT1-modified MSCs can specifically reverse the expression of Penitrem A, a finding that provides new ideas for metabolically targeted anti-aging interventions.

In delving deeper into the mysteries of cross-species development, our preliminary research has lifted a corner of the veil on epigenetics, revealing its magnificent landscape characterized by both rapid fluctuations and enduring constants across the vast expanse of evolutionary time. Notably, the emergence of super-enhancers as a stable cornerstone represents a significant breakthrough in this field⁴⁹. Building on this momentum, our current study shifts focus to the diverse chapters of the mammalian life journey, from tender infancy to the depths of aging, meticulously portraying the grand narrative of development and senescence. In this study, in addition to super-enhancers, we discovered a series of bridges that connect stability and change, youth and aging. The dynamic adjustments of cell populations, mitochondrial markers, and metabolic markers together weave a complex network of the mammalian life cycle. Our results deepen our understanding of the central roles in mammalian development and aging and enrich our understanding of the mechanisms of aging in life. Future research should focus on two key directions: first, developing artificial intelligence-driven aging prediction models that integrate the cross-omics biomarker systems established in this study to break through the limitations of single-species research; second, the validity and generalizability of the system in pet dogs (home environment) and working dogs (high stress environment) were evaluated by a Randomized controlled trial system. The collaborative advancement of the above work will accelerate the leap of canine aging research from mechanism analysis to translational medicine application, and provide a cross-species theoretical framework and technical platform for the development of personalized anti-aging strategies.

Methods

Animals

A total of 19 dogs were used in this study. Among them, 15 police dogs were obtained from Shanghai Zhongbao Hua'an Longgen Special Dog Company and used for the acquisition of aging biomarkers and anti-aging research. Sex and sign information for all dogs is described in Table 1. In this study, stratified random sampling was used to group all dogs in order to reduce the impact of dog breeds. All dogs were divided into 5 groups, NC Group (4 dogs), MSCs group (4 dogs), NMNAT1-MSCs group (4 dogs), young control group (3 dogs), and test group (4 dogs). Dogs numbered 2-1 (12 years old), 2-2 (6 years old), and 6-1 (3 years old) were used to collect PBMCs for single-cell transcriptome sequencing. Four dogs were recruited from volunteers, with ages of 1, 8, 8, and 12 years old, respectively. These four volunteer dogs were used for the evaluation of aging biomarkers. None of the dogs had undergone sterilization surgery. Before collecting whole blood for subsequent research, the dogs were fasted for 8 hours. The animal study protocol was approved by the Northwest A&F University animal care and use committee (ACUC), protocol number [IAUC2024-1109]. We have complied with all relevant ethical regulations for animal use. The work has been reported in line with the ARRIVE guidelines 2.0. All experimental

protocols were carried out according to the guidelines established by the Chinese National Standard GB/T35892-2018 (guidelines for the ethical review of laboratory animal welfare), submitted and previously approved by the Ethics Committee on the Use of Animals of the Northwest A&F University.

Isolation of peripheral blood mononuclear cells (PBMCs)

First, whole blood from a dog is collected into EDTA-coated blood collection tubes. Following the manufacturer's instructions (Tianjin Haoyang Huake Biotechnology Co., Ltd. LDS1077), an equal volume of PBS (half of the total blood volume) is used to dilute the blood, and then an equal volume of separation medium is added. The mixture is centrifuged at 500 g for 25 minutes at 20 °C. The second layer of creamy white cells, located just above the red blood cell layer, is carefully aspirated. After adding 10 mL of wash buffer and mixing thoroughly, the suspension is centrifuged at 250 g for 10 minutes⁵⁰. The supernatant is discarded, leaving the precipitate as the PBMCs.

Single cell library construction and sequencing

The single-cell RNA library construction and sequencing were performed following established protocols⁵¹. Briefly, cellular suspensions were loaded onto a 10X Genomics GemCode Single-cell instrument to generate single-cell Gel Bead-In-Emulsions (GEMs), and libraries were prepared using Chromium Next GEM Single Cell 3' Reagent Kits v3.1. Upon Gel Bead dissolution within a GEM, primers containing an Illumina® R1 sequence, a 16 nt 10x Barcode, a 10 nt Unique Molecular Identifier (UMI), and a poly-dT primer sequence were released, mixing with cell lysate and MasterMix to enable reverse transcription of poly-adenylated mRNA into barcoded, full-length cDNAs. Following this, silane magnetic beads were employed to clean up the post-GEM reaction mixture by removing leftover biochemical reagents and primers, and the full-length, barcoded cDNAs were then amplified by PCR to generate sufficient mass for library construction. The library construction phase involved adding P5, P7, a sample index, and the R2 (read 2 primer sequence) to the molecules (with R1 having been incorporated during GEM incubation) via processes including End Repair, A-tailing, Adaptor Ligation, and PCR, ensuring the final libraries contained the P5 and P7 primers necessary for Illumina bridge amplification. Finally, these Single Cell 3' Protocol-produced Illumina-ready sequencing libraries, which are standard Illumina paired-end constructs beginning and ending with P5 and P7, were sequenced; Read 1 encoded the 16 bp 10x Barcode and 10 bp UMI, Read 2 was used to sequence the cDNA fragment, and sample index sequences were incorporated as the i7 index read, with Read 1 and Read 2 serving as standard Illumina® sequencing primer sites.

Preprocess of scRNA-seq data

The raw sequencing data files were processed using Cell Ranger (version 8.0, 10x Genomics) and mapped to the CanFam3.1(Ensembl release 104) reference genome. Expression matrices were subsequently generated for downstream analysis. For each sample, the count matrix was imported into the Seurat³⁰ pipeline using Read10X function. To determine the quality of the data, the percentage of reads mapped to mitochondrial chromosomes was calculated per cell using the PercentageFeatureSet function, setting the 'pattern' parameter to '^MT-'. Quality control measures were applied to all samples. Cells meeting the following criteria were retained for downstream analysis: (1) 200 < nFeature_RNA < 4000. (2) percent.mt < 10. (3) 500 < nCount_RNA < 30000. Next, all samples were normalized using SCTransform⁵². Subsequently, Harmony³¹ was applied to remove the batch effects.

Cell type annotation

The neighbor graph of cells was constructed using the first 50 Harmony components with the FindNeighbors () function. The Leiden³² algorithm, with a resolution of 1.6, was then applied to the KNN graph, resulting in the clustering of cells into 31 clusters. To identify marker genes for each cluster, the FindAllMarkers () function was used. Cell types were annotated by referencing cell type markers for canine PBMC, assigning each cluster to a

Table 1 | Dog information

Sample ID	Breed	Sex	Age	group	Height (cm) (vertical distance from the highest point of the shoulder crest to the ground)	Body length (cm) (distance from point of shoulder to outer edge of rump end)	Weight (kg)
1-1	Beagle	Male	6	NC	35	42	29
1-2	Beagle	Male	10	NC	32	40	26.1
1-3	Belgian Malinois	Male	8	NC	51	44	45.4
1-4	Belgian Malinois	Male	8	NC	48	41	40.8
2-1	Beagle	Female	12	MSCs	32	38	12.15
2-2	Beagle	Female	6	MSCs	30	40	14.5
2-3	Labrador	Male	8	MSCs	53	43	36.8
2-4	Springer Spaniel	Female	8	MSCs	37	46	18.6
4-1	Beagle	Female	10	NMNAT1-MSCs	34	43	26.4
4-2	Beagle	Male	8	NMNAT1-MSCs	36	44	21.7
4-3	Springer Spaniel	Female	8	NMNAT1-MSCs	38	40	20.9
4-4	Beagle	Male	8	NMNAT1-MSCs	37	44	18
6-1	Beagle	Female	3	Con	30	34	19.1
6-2	Beagle	Female	3	Con	33	32	15.7
6-3	Beagle	Female	3	Con	34	29	19.4
test1	mongrel	Male	1	test	25	31	15.4
test2	mongrel	Male	8	test	29	33	21.5
test3	mongrel	Female	8	test	34	39	23.4
test4	mongrel	Female	12	test	28	33	18.9

A description of the detailed physiological information of the dogs participating in the experiment.

corresponding cell type based on the specific high expression of certain markers. The cell type markers for this study are: CD8+ T cells/NK cells (CCL5, GZMB, KLRB1, NCR3, GZMA, IL12RB2, KLRK1, KLRD1 and CD96), CD4+ T cells (IL7R, LEF1, DOCK3, ATP10A, CD52, CSTA, ICOS and CD3E), neutrophils (S100A12, CYP4F22, SGK1, IL1R2 and S100A8), B cells (TNFRSF13C, PAX5, EBF1, BTLA, NRIP1, MS4A1 and PLEKHO1), plasma cells (JCHAIN, TXNDC5, IRF4, TNFRSF17, DERL3, CCR10, TNFRSF13B, MZB1, LMAN1, LAP3 and RARRES2), polymorphonuclear myeloid-derived suppressor cells (PMN-MDSCs) (CAMP, PGLYRP1, CRISP2, MMP9, MMP8, TCN1, LTF and FADS1), platelets (PPBP) (Supplementary Fig. 1c, d), eosinophils/basophils (C30H15orf48, TGM2, SLCO4C1, SMPD1, ADGRE2, CSTB, DACH1, CA8, IL5RA and DAPK2) and monocytes/DCs (LYZ, MAFB, BPI, FN1, F13A1, TCF7L2, CD83, NRG1, PLXDC2, MITF, RETN, SLAMP9, TCF4 and HAVCR1).

Identification of immature neutrophils

Cell trajectory and function enrichment analyses were employed to identify immature neutrophils. We used Monocle³⁴ to construct the neutrophil developmental trajectory. CytoTRACE2³⁵ was applied to predict cell differentiation potential and determine the starting point of the trajectory. Additionally, UCell³⁶ was utilized to score all neutrophils based on KEGG⁵³ functional annotation to further characterize their molecular profiles.

Cell correlation analysis

We identified temporally dynamic cell types by analyzing pseudo-bulk gene expression profiles across three time points. Briefly, single-cell transcriptomes were aggregated into pseudo-bulk profiles for each cell type using Seurat's Average Expression function, generating a representative expression matrix per time point. Pearson correlations were then computed

between all pairwise combinations of these time-resolved pseudo-bulk profiles (Age 3 vs. Age 6, Age 3 vs. Age 12, Age 6 vs. Age 12). Cell types exhibiting a correlation coefficient $r < 0.95$ in any pairwise comparison were classified as age-related, whereas those maintaining $r \geq 0.95$ across all three time points were considered temporally stable.

Cellular potency score

We employed CytoTRACE2 to predict cellular potency scores. This tool predicts differentiation potential by analyzing the diversity of gene expression within individual cells. Its core principle states that undifferentiated high-potency cells (e.g., stem cells) broadly express a diverse range of genes, whereas terminally differentiated mature cells exhibit specialized and restricted gene expression patterns. Furthermore, the algorithm was trained on cross-tissue and cross-species single-cell datasets, enabling it to identify universal patterns associated with developmental potential (such as specific gene combinations commonly active in stem cells). These patterns were then translated into an interpretable scoring model. Each cell is ultimately assigned a continuous score ranging from 0 (terminally differentiated) to 1 (totipotent), where higher values indicate greater differentiation potential. For instance, totipotent cells score near 1 due to their extensive expression of housekeeping genes, while terminally differentiated cells approach 0 as their gene expression becomes highly specialized. This scoring system facilitates stem cell identification, developmental trajectory tracing, and comparative analysis of cellular potency across different physiological or pathological states.

LC-MS/MS Analysis

For metabolomic profiling, LC-MS/MS analysis was conducted based on previously reported methods⁵⁴. Sample analysis was conducted at Shanghai Applied Protein Technology Co., Ltd., employing a Thermo Vanquish

UHPLC system coupled to an Orbitrap mass spectrometer. For HILIC separation, a Waters ACQUITY UPLC BEH Amide column (1.7 μm , 2.1 \times 100 mm) was utilized. The mobile phase, used in both ESI positive and negative modes, consisted of A (25 mM ammonium acetate and 25 mM ammonium hydroxide in water) and B (acetonitrile). The gradient elution started at 98% B for 1.5 min, linearly decreased to 2% B over 10.5 min, held for 2 min, returned to 98% B in 0.1 min, and concluded with a 3-min re-equilibration. ESI source parameters were set to Gas1: 60, Gas2: 60, CUR: 30, source temperature: 600 $^{\circ}\text{C}$, and ISVF: ± 5500 V. Full MS scans (MS1) were acquired from m/z 80–1200 at 60,000 resolution with a 100 ms accumulation time. Auto MS/MS acquisitions covered m/z 70–1200 at 30,000 resolution with a 50 ms accumulation time and a 4-second dynamic exclusion.

Preprocess of Plasma metabolomic data

ProteoWizard MSConvert⁵³ was applied to convert the raw MS data into MzXML files and then subjected to peak picking and grouping using XCMS⁵⁵ with parameter: centWave $m/z = 10$ ppm, peak width = $c(10,60)$, prefilter = $c(10,100)$, bw = 5, $mz\text{wid} = 0.025$, minfrac = 0.5. Additionally, CAMERA⁵⁶ was used to annotate the isotopes and adducts. Only extracted ion features with more than 50% of the non-zero values in all samples were kept. Compound identification of metabolites was performed by comparing of accuracy m/z value (<10 ppm), and MS/MS spectra with an in-house database established with available authentic standards (Shanghai Applied Protein Technology Co. Ltd).

Identification of age-related metabolites

Correlation analysis between metabolites and age was performed using the pcor.test function of the ppcor package⁵⁷ (version 1.1) via the Spearman correlation method. Metabolites significantly related to age were then clustered into six groups using the fuzzy C-means clustering method⁵⁸ provided by the R package Mfuzz⁵⁹. Functional enrichment for each cluster was subsequently performed using the KEGG⁵³ database.

Evaluation of stem-cell therapy

Gene set variation analysis (GSVA)⁶⁰ was applied to evaluate both natural aging samples and two different stem cell therapy samples, using age-related metabolites.

Preprocess of bulk RNA-Seq data

Quality control was performed using Fastp⁶¹ with default parameters. Clean reads were mapped to the CanFam3.1 reference genome (Ensembl release 104) with HISAT2⁶², and reads with a mapping quality over 20 were counted for gene expression quantitation using featureCounts⁶³. Transcript per million (TPM) values were calculated using a custom R script.

Preprocess of proteomic data

Raw files were searched against the Uniprot database using Proteome Discoverer⁶⁴ with the following parameters: a mass tolerance of 10 ppm for precursor ions and 0.02 Da for product ions. Carbamidomethylation was set as a fixed modification, while oxidation of methionine (M) and N-terminal methionine loss were set as dynamic modifications. Up to 2 missed cleavage sites were allowed. To ensure high-quality results, Peptide Spectrum Matches (PSMs) with a credibility of over 99% were identified and retained. Identified proteins containing at least one unique peptide were included, with a false discovery rate (FDR) of no more than 1.0%.

Functional enrichment analysis

Functional enrichment analysis for genes, proteins, and metabolites was conducted using the R package ClusterProfiler⁶⁵ with GO⁶⁶ and KEGG⁵³ databases. Additionally, gene set enrichment analysis (GSEA)⁶⁷ was performed for metabolites using markers from the Aging Atlas⁶⁸.

Cellular communication analysis

Cell Chat³⁹ was utilized for the purpose of conducting cell communication analysis^{69,70}. The receptor-ligand pairs utilized for secreted signaling, ECM-

receptor interactions, cell-cell contact, and non-protein signaling were employed for further analysis, with the source cells participating in communication restricted to two types of MDSCs: M-MDSC and PMN-MDSC. The overall information flow of each signal pathway was analyzed, defined as the sum of communication probabilities between all pairs of cell populations in the network (i.e., the total weight of the network). Subsequently, this study compared the communication probabilities of ligand-receptor pair regulation from MDSCs to other immune cells.

Isolation and culture of dog mesenchymal stem cells

MSCs were derived from the abdominal subcutaneous adipose tissue of two 6-month-old female hybrid dogs. The detailed MSCs separate steps and MSCs identification were described in our previous report⁷¹. Fat tissue was obtained subcutaneously from the abdomen by surgery, and then cut into pieces after removal of blood vessels and fascia. A-mem medium containing 0.1% collagenase type I was used to digest adipose tissue, placed at 37 $^{\circ}\text{C}$ in a 5% CO_2 incubator for 1 H. The upper liquid was removed after centrifugation at 1000 rpm/min for 5 min. The pelleted cells were resuspended in a-MEM with 10% FBS, mounted in a dish, and incubated in a 5% CO_2 incubator at 37 $^{\circ}\text{C}$. The cells were cultured in α -MEM (Invitrogen, Carlsbad, CA) complete medium at 37 $^{\circ}\text{C}$, 5% CO_2 incubator. When the cells were attached to the bottom of the plate at about 80%, a 1:3 passage was performed. Treated and used the 3–9 passage cells. To establish a model of cellular senescence, we used serial passages up to the 9 passage to obtain different degrees of cellular senescence, referring to previous methods^{22–26,28,29}.

Establishment of NMNAT1 Overexpressing MSCs

Consistent with our previously reported methods, MSCs overexpressing NMNAT1 have been established²⁸. Based on the canine NMNAT1 gene sequence (XM_038666674.1) from the NCBI database, cloning primers were designed and synthesized. The cloning primer sequences for NMNAT1 are provided in Supplemental data 1. RNA was extracted from canine MSCs and reverse-transcribed (Thermo Scientific, USA) to obtain cDNA. PCR reactions were performed using this cDNA template and high-fidelity enzymes (Takara, Japan) to clone NMNAT1. The correct band was obtained via 1% agarose gel electrophoresis and recovered using a gel extraction kit (Tiangen, China).

The pCDH-CMV-MCS-EF1-copGFP-T2APuro vector was utilized for constructing the NMNAT1 overexpression vector. EcoR I (upstream) (Takara, Japan) and BamH I (downstream) (Takara, Japan) were selected as the restriction enzyme sites, and the vector backbone and NMNAT1 recovered fragment were digested using QuickCut restriction enzymes (Takara, Japan). The recovered products were then purified using a gel extraction kit (Tiangen, China). The purified products were ligated to the vector backbone using T4 DNA ligase (Thermo Scientific, USA). The ligation mixture was mixed with DH5 α (QINGKE, China) competent cells on ice and subjected to heat shock at 42 $^{\circ}\text{C}$ for 90 seconds, followed by immediate transfer to ice. The bacterial suspension was evenly spread onto an LB agar plate containing ampicillin and incubated overnight at 37 $^{\circ}\text{C}$ in an inverted position. A single positive colony was picked and sent for sequencing (QINGKE, China). The bacterial culture with 100% correct sequencing was expanded in 15 mL of LB broth containing ampicillin and shaken overnight at 37 $^{\circ}\text{C}$. Plasmids were extracted using a plasmid extraction kit (Tiangen, China).

When 293 T cells reached 80% confluence, 500 μL of Opt-MEM/DM (Gibco, USA), 18 μL of PEI (Thermo Fisher, USA), and 6 μg of plasmid were added and mixed for transfection. After 12 hours, the medium was replaced with 4 mL of DMEM (+), and the cells were continuously cultured for 48 hours. The culture medium rich in lentivirus was then collected. The collected supernatant was centrifuged at 2000 rpm for 5 minutes, and the supernatant was transferred to a new tube.

When the MSC density reached 20–40%, the infection experiment was performed. Fresh culture medium was mixed with the lentiviral supernatant in a 1:1 ratio, and 3 μL of polybrene (Thermo Fisher, USA) was added. After

12 hours, the medium was replaced with fresh culture medium, and fresh medium was exchanged every 24 hours thereafter.

MSCs transplantation intervenes in aging

12 dogs were divided into 3 groups, including the MSCs group, the NMNAT1-MSCs group, and the aged control group (Table 1). The average age of the intervention dogs was 7 years, and all the intervention dogs were retired due to a decline in working performance. The MSCs group and the NMNAT1-MSCs group received intravenous injections of MSCs and NMNAT1-MSCs (1×10^7 per dog, dissolved in saline) via the cephalic vein on days 1 and 30, respectively. The control group received intravenous injections of an equal volume of saline via the cephalic vein on days 1 and 30. Blood samples were collected on days 0, 30, and 60 for hematological and serum biochemical analyses. On day 60, serum was collected for metabolomics analysis. In this study, the personnel who raised and treated the dogs and the data collection personnel were different. In all experiments, the data collectors were blinded to the grouping.

Flow cytometry analysis

Firstly, adjust the cell suspension to a concentration of 1×10^7 cells/mL. According to the supplier's instructions, add antibodies and mix thoroughly (tdscience, China). Incubate the mixture in the dark at 4 °C for 30 minutes. Centrifuge at 300–400 g for 5 minutes, discard the supernatant, and resuspend the PBMCs in 1 mL of solution. For PBMC sorting, PBMCs are incubated with CD3/CD4/CD8 antibodies (Bio-Rad, TC014, 1:100) and sorted by flow cytometry using FACSAria™ III (BD, USA).

For MSCs, the Mitochondrial Membrane Potential Assay Kit with Apoptosis Detection (Beyotime, C1071S) and the Live Cell Caspase-3 Activity Assay Kit with Annexin V Apoptosis Detection (Beyotime, C1077S) are used to detect cellular changes. Following the manufacturer's protocol, mix the dyes with the cells and incubate in the dark at room temperature for 20 minutes. Analyze the samples on a CytoFLEX (Beckman Coulter, USA), and use CytExpert 2.3.0.84 to analyze the results⁷². FSCs and SSCs are used to plot dot plots to identify intact individual cells. For each staining channel, set the groups to be separately stained. Gating strategy is confirmed by Flow cytometry histograms of dye abundances (Supplementary Fig. 6a, b).

Quantitative Real-Time PCR (QRT-PCR) analysis

According to the manufacturer's instructions, the total RNA of cells was extracted by Trizol reagent (Takara, Japan), and reverse transcriptase reagent kit (Thermo Scientific, USA) was used. QRT-PCR was carried out with the CFX96 Real-Time PCR system (Bio-Rad, USA) as follows: pre-denaturation at 94 °C for 5 min, following 39 cycles for 30 s at 94 °C, annealing for 30 s at 58 °C and 30 s at 70 °C for extending. β -Actin was used as an internal control. Comparative CT-values from QPCR were used to measure relative gene expression⁷³. Primers are listed in Supplementary data 1.

Giemsa staining

According to the manufacturer's instructions (Beyotime, CHINA), the stock solution of Giemsa stain is diluted tenfold with deionized water. Discard the residual culture medium in the cell culture plate, wash the cells with PBS, and fix them with 4% paraformaldehyde for 5 minutes. Subsequently, add the prepared Giemsa stain solution, allow it to stand at room temperature for 15 minutes, and then discard the stain solution⁷⁴. Wash the cells twice with PBS. Add an appropriate amount of PBS to the culture plate and observe and photograph the cells under a microscope.

β -Galactosidase staining

According to the manufacturer's instructions (Beyotime, CHINA), aspirate the cell culture medium and wash the cells once with PBS. Add 1 mL of β -galactosidase staining fixative and fix the cells at room temperature for 15 minutes⁷⁵. After discarding the fixative, wash the cells

three times with PBS, and add the staining solution for incubation overnight at 37 °C.

Immunofluorescence staining

Cells were seeded on cell slides and fixed with 4% paraformaldehyde when the confluence reached 60%. According to the manufacturer's instructions, Lamin B1 (CST, USA, 1:100) was added to the cell culture plate and incubated overnight at 4 °C⁷⁶. After incubation, the antibody was washed away, and a fluorescently labeled goat anti-rabbit secondary antibody (ZHONGSHANJINQIAO, CHINA, 1:500) was added and incubated in the dark for 1 hour. Before observation, Hoechst 33342 (Beyotime, CHINA, 1:1000) at 0.5 μ g/mL was used to stain the cells for 5 minutes. The samples were observed and photographed under a laser scanning confocal microscope (Leica, Germany). Image processing using LAS X 4.7.0.

Blood routine and biochemical analysis

For blood routine collection and analysis, whole blood samples from dogs were collected using anticoagulant tubes containing EDTA. For blood biochemical data, whole blood samples from dogs were collected using anticoagulant tubes without EDTA. The blood routine and biochemical analysis of dogs were completed by the Zoetis Shanghai Laboratory. All blood routine data are presented in Supplemental Data 2. All blood biochemical data are presented in Supplementary data 3.

Western blot

The western blotting protocols followed our previous study⁷³. MSCs were collected with NP40 lysis buffer (Beyotime, China) containing phosphatase and protease inhibitors. Proteins were collected from the cell lysates after centrifugation at 12,000 r/min for 20 min at 4 °C. After concentration determination using the Bradford assay (Tiangen Biotech, PA102, China), proteins were denatured in loading buffer, followed by separation using sodium dodecyl sulfate-polyacrylamide gel electrophoresis (SDS-PAGE)⁷⁷. NMNAT1 (Immunway, USA, 1:1000), p16 (proteintech, CHINA, 1:2000), p53 (proteintech, CHINA, 1:50000), LAMINB1 (CST, USA, 1:1000) were used to detect the expression of related proteins. The results were detected using a Tanon 4600SF automatic chemiluminescence image analysis system (Tanon, CHINA). Uncropped blots photographs are shown in Supplementary Figs. 8–10.

Statistics and reproducibility

For bioinformatic analyses, single-cell RNA sequencing (scRNA-seq) data were preprocessed in R (version 4.2.3) included: quality control, normalization (SCTransform), batch effect correction (Harmony), clustering (Leiden algorithm), and marker gene identification using the Wilcoxon sum rank test. For proteomic and metabolomic data, raw reads were log-transformed and median-normalized, and differentially expressed proteins/metabolites were identified using the Wilcoxon rank-sum test. As for transcriptomic data, differentially expressed genes were identified using negative binomial test provided by DESeq2 (version 1.48.1)⁷⁸.

All experiments were independently replicated at least 3 times, with cells from a single isolate used for each experiment. When the main effects were significant, one-way analysis of variance (ANOVA) was used, followed by Newman–Keuls multiple range tests. The student's t-test was used when comparing the means of two groups. All the data are presented as mean \pm SD, and statistical significance are shown as follows: * $p < 0.05$; ** $p < 0.01$; *** $p < 0.001$, **** $p < 0.0001$. All data were analysed using GraphPad Prism 8.4.3 software (La Jolla, CA, USA) and ImageJ 1.8.0 (National Institutes of Health, USA), each set contained at least 3 different replicates.

Reporting summary

Further information on research design is available in the Nature Portfolio Reporting Summary linked to this article.

Data availability

The raw sequence data reported in this paper have been deposited in the Genome Sequence Archive (Genomics, Proteomics & Bioinformatics 2021) in National Genomics Data Center (Nucleic Acids Res 2022), China National Center for Bioinformation / Beijing Institute of Genomics, Chinese Academy of Sciences (GSA: CRA025543) that are publicly accessible at <https://ngdc.cnbc.ac.cn/gsa>. The proteomics and metabolomics data reported in this paper have been deposited at the National Bioinformatics Center of the National Genomics Institute of China/Beijing Genomics Institute (OMIX: Accession Number OMIX010110; OMIX010111; OMIX010212). All data generated and analyzed during this study are included in this published article and supplementary information.

Code availability

The R scripts for bioinformatics analysis are available at https://github.com/ch31lyDim/Multiomics_dog_aging.

Received: 18 November 2024; Accepted: 3 June 2025;

Published online: 10 June 2025

References

- López-Otín, C., Blasco, M. A., Partridge, L., Serrano, M. & Kroemer, G. Hallmarks of aging: An expanding universe. *Cell* **186**, 243–278 (2023).
- Han, J. J. The ticking of aging clocks. *Trends Endocrinol. Metab.* **35**, 11–22 (2024).
- Creevy, K. E., Akey, J. M., Kaeberlein, M. & Promislow, D. E. L. An open science study of ageing in companion dogs. *Nature* **602**, 51–57 (2022).
- Leslie, M. Massive study of dog aging likely to lose funding. *Science* **383**, 137–138 (2024).
- Hoffman, J. M., Creevy, K. E., Franks, A., O'Neill, D. G. & Promislow, D. E. L. The companion dog as a model for human aging and mortality. *Aging Cell* **17**, e12737 (2018).
- Wang, T. et al. Quantitative translation of dog-to-human aging by conserved remodeling of the DNA Methylome. *Cell Syst.* **11**, 176–185.e176 (2020).
- Jiménez, A. G. A revisiting of “the hallmarks of aging” in domestic dogs: current status of the literature. *Geroscience* **46**, 241–255 (2024).
- Alcorta, D. A. et al. Involvement of the cyclin-dependent kinase inhibitor p16 (INK4a) in replicative senescence of normal human fibroblasts. *Proc. Natl Acad. Sci. USA* **93**, 13742–13747 (1996).
- Hall, B. M. et al. p16(Ink4a) and senescence-associated β -galactosidase can be induced in macrophages as part of a reversible response to physiological stimuli. *Aging* **9**, 1867–1884 (2017).
- Frescas, D. et al. Murine mesenchymal cells that express elevated levels of the CDK inhibitor p16(Ink4a) in vivo are not necessarily senescent. *Cell Cycle* **16**, 1526–1533 (2017).
- Yosef, R. et al. p21 maintains senescent cell viability under persistent DNA damage response by restraining JNK and caspase signaling. *EMBO J.* **36**, 2280–2295 (2017).
- Wang, L. et al. Targeting p21(Cip1) highly expressing cells in adipose tissue alleviates insulin resistance in obesity. *Cell Metab.* **34**, 75–89.e78 (2022).
- He, Y. et al. 4E-BP1 counteracts human mesenchymal stem cell senescence via maintaining mitochondrial homeostasis. *Protein Cell* **14**, 202–216 (2023).
- Zhu, Y. et al. The Achilles' heel of senescent cells: from transcriptome to senolytic drugs. *Aging Cell* **14**, 644–658 (2015).
- Williams, P. A. et al. Vitamin B(3) modulates mitochondrial vulnerability and prevents glaucoma in aged mice. *Science* **355**, 756–760 (2017).
- Yasuda, I. et al. Pre-emptive short-term nicotinamide mononucleotide treatment in a mouse model of diabetic nephropathy. *J. Am. Soc. Nephrol.* **32**, 1355–1370 (2021).
- Fang, E. F. et al. NAD(+) augmentation restores mitophagy and limits accelerated aging in Werner syndrome. *Nat. Commun.* **10**, 5284 (2019).
- Fang, E. F. et al. NAD(+) in Aging: Molecular mechanisms and translational implications. *Trends Mol. Med.* **23**, 899–916 (2017).
- Verdin, E. NAD⁺ in aging, metabolism, and neurodegeneration. *Science* **350**, 1208–1213 (2015).
- Lautrup, S. et al. Decreased mitochondrial NAD⁺ in WRN deficient cells links to dysfunctional proliferation. *Aging*, <https://doi.org/10.18632/aging.206236> (2025).
- Zeng, M. et al. Transcriptomic and intervention evidence reveals domestic dogs as a promising model for anti-inflammatory investigation. *Aging Cell* **23**, e14127 (2024).
- Kapetanios, K., Asimakopoulos, D., Christodoulou, N., Vogt, A. & Khan, W. Chronological age affects MSC senescence in vitro—a systematic review. *Int J. Mol. Sci.* **22**, 7945 (2021).
- Siennicka, K., Zołocińska, A., Dębski, T. & Pojda, Z. Comparison of the donor age-dependent and in vitro culture-dependent mesenchymal stem cell aging in rat model. *Stem Cells Int.* **2021**, 6665358 (2021).
- Babenko, V. A. et al. Age-related changes in bone-marrow mesenchymal stem cells. *Cells* **10**, <https://doi.org/10.3390/cells10061273> (2021).
- Wang, B. et al. Transplanting cells from old but not young donors causes physical dysfunction in older recipients. *Aging Cell* **19**, e13106 (2020).
- Lu, G. M. et al. Multiomics global landscape of stemness-related gene clusters in adipose-derived mesenchymal stem cells. *Stem Cell Res Ther.* **11**, 310 (2020).
- Gao, Y. et al. Multi-omics analysis of human mesenchymal stem cells shows cell aging that alters immunomodulatory activity through the downregulation of PD-L1. *Nat. Commun.* **14**, 4373 (2023).
- Li, C. et al. SPARC overexpression in allogeneic adipose-derived mesenchymal stem cells in dog dry eye model induced by benzalkonium chloride. *Stem Cell Res Ther.* **15**, 195 (2024).
- Jing, Y. et al. Mesenchymal stem cells with simultaneous overexpression of GPX3 and CD47 for the treatment of drug-induced acute liver injury. *Vet. Sci.* **12**, <https://doi.org/10.3390/vetsci12020149> (2025).
- Hao, Y. et al. Dictionary learning for integrative, multimodal and scalable single-cell analysis. *Nat. Biotechnol.* **42**, 293–304 (2024).
- Korsunsky, I. et al. Fast, sensitive and accurate integration of single-cell data with Harmony. *Nat. Methods* **16**, 1289–1296 (2019).
- Traag, V. A., Waltman, L. & van Eck, N. J. From Louvain to Leiden: guaranteeing well-connected communities. *Sci. Rep.* **9**, 5233 (2019).
- Wu, H. et al. Mapping the single-cell transcriptomic response of murine diabetic kidney disease to therapies. *Cell Metab.* **34**, 1064–1078.e1066 (2022).
- Qiu, X. et al. Reversed graph embedding resolves complex single-cell trajectories. *Nat. Methods* **14**, 979–982 (2017).
- Kang, M. et al. Mapping single-cell developmental potential in health and disease with interpretable deep learning. *bioRxiv*, <https://doi.org/10.1101/2024.03.19.585637> (2024).
- Andreatta, M. & Carmona, S. J. UCell: Robust and scalable single-cell gene signature scoring. *Comput. Struct. Biotechnol. J.* **19**, 3796–3798 (2021).
- Sadiqu, P. et al. Neutrophils fuel effective immune responses through gluconeogenesis and glycogenesis. *Cell Metab.* **33**, 411–423.e414 (2021).
- Li, J. et al. Determining a multimodal aging clock in a cohort of Chinese women. *Med.* **4**, 825–848.e813 (2023).
- Jin, S. et al. Inference and analysis of cell-cell communication using CellChat. *Nat. Commun.* **12**, 1088 (2021).
- Consortium, A. A. Aging Atlas: a multi-omics database for aging biology. *Nucleic Acids Res.* **49**, D825–D830 (2021).

41. Ammons, D. T. et al. Single-cell RNA sequencing reveals the cellular and molecular heterogeneity of treatment-naïve primary osteosarcoma in dogs. *Commun. Biol.* **7**, 496 (2024).
42. Ammons, D. T. et al. A single-cell RNA sequencing atlas of circulating leukocytes from healthy and osteosarcoma affected dogs. *Front. Immunol.* **14**, 1162700 (2023).
43. Chen, H. et al. Adherence to Life's Essential 8 is associated with delayed biological aging: a population-based cross-sectional study. *Rev. Esp. Cardiol. (Engl. Ed.)* **78**, 37–46 (2025).
44. Qiu, J. et al. Ucp1 ablation improves skeletal muscle glycolytic function in aging mice. *Adv. Sci.* **12**, e2411015 (2025).
45. Li, G. J. et al. Downregulation of NAD Kinase Expression in β -cells contributes to the aging-associated decline in glucose-stimulated insulin secretion. *Aging Cell*, e70037, <https://doi.org/10.1111/accel.70037> (2025).
46. Huang, X. et al. The relationship between telomere length and aging-related diseases. *Clin. Exp. Med.* **25**, 72 (2025).
47. Vasudevarao, M. D. et al. BMP signaling promotes zebrafish heart regeneration via alleviation of replication stress. *Nat. Commun.* **16**, 1708 (2025).
48. de Magalhães, J. P. Distinguishing between driver and passenger mechanisms of aging. *Nat. Genet.* **56**, 204–211 (2024).
49. Yang, Y. et al. Metformin decelerates aging clock in male monkeys. *Cell* **187**, 6358–6378.e6329 (2024).
50. Razmara, A. M. et al. Preclinical evaluation and first-in-dog clinical trials of PBMC-expanded natural killer cells for adoptive immunotherapy in dogs with cancer. *J. Immunother. Cancer* **12**, <https://doi.org/10.1136/jitc-2023-007963> (2024).
51. Hu, W. et al. Single-cell RNA sequencing dissects the immunosuppressive signatures in *Helicobacter pylori*-infected human gastric ecosystem. *Nat. Commun.* **16**, 3903 (2025).
52. Hafemeister, C. & Satija, R. Normalization and variance stabilization of single-cell RNA-seq data using regularized negative binomial regression. *Genome Biol.* **20**, 296 (2019).
53. Kanehisa, M., Furumichi, M., Sato, Y., Kawashima, M. & Ishiguro-Watanabe, M. KEGG for taxonomy-based analysis of pathways and genomes. *Nucleic Acids Res.* **51**, D587–D592 (2023).
54. Wang, L. et al. To explore the mechanism of acupoint application in the treatment of primary dysmenorrhea by 16S rDNA sequencing and metabolomics. *Front. Endocrinol.* **15**, 1397402 (2024).
55. Forsberg, E. M. et al. Data processing, multi-omic pathway mapping, and metabolite activity analysis using XCMS Online. *Nat. Protoc.* **13**, 633–651 (2018).
56. Kuhl, C., Tautenhahn, R., Böttcher, C., Larson, T. R. & Neumann, S. CAMERA: an integrated strategy for compound spectra extraction and annotation of liquid chromatography/mass spectrometry data sets. *Anal. Chem.* **84**, 283–289 (2012).
57. Kim, S. ppcor: An R Package for a fast calculation to semi-partial correlation coefficients. *Commun. Stat. Appl Methods* **22**, 665–674 (2015).
58. Bezdek, J. C., Ehrlich, R. & Full, W. FCM: The fuzzy c-means clustering algorithm. *Comput. Geosci.* **10**, 191–203 (1984).
59. Kumar, L. & M, E. F. Mfuzz: a software package for soft clustering of microarray data. *Bioinformatics* **2**, 5–7 (2007).
60. Hänzelmann, S., Castelo, R. & Guinney, J. GSVA: gene set variation analysis for microarray and RNA-seq data. *BMC Bioinforma.* **14**, 7 (2013).
61. Chen, S., Zhou, Y., Chen, Y. & Gu, J. fastp: an ultra-fast all-in-one FASTQ preprocessor. *Bioinformatics* **34**, i884–i890 (2018).
62. Kim, D., Paggi, J. M., Park, C., Bennett, C. & Salzberg, S. L. Graph-based genome alignment and genotyping with HISAT2 and HISAT-genotype. *Nat. Biotechnol.* **37**, 907–915 (2019).
63. Liao, Y., Smyth, G. K. & Shi, W. featureCounts: an efficient general purpose program for assigning sequence reads to genomic features. *Bioinformatics* **30**, 923–930 (2014).
64. Orsburn, B. C. Proteome discoverer—a community enhanced data processing suite for protein informatics. *Proteomes* **9**, 15 (2021).
65. Wu, T. et al. clusterProfiler 4.0: A universal enrichment tool for interpreting omics data. *Innovation* **2**, 100141 (2021).
66. The Gene Ontology Resource: 20 years and still GOing strong. *Nucleic Acids Res.* **47**, D330–D338, (2019).
67. Subramanian, A. et al. Gene set enrichment analysis: a knowledge-based approach for interpreting genome-wide expression profiles. *Proc. Natl Acad. Sci. USA* **102**, 15545–15550 (2005).
68. Aging Atlas: a multi-omics database for aging biology. *Nucleic Acids Res.* **49**, D825–D830, (2021).
69. Chen, W. B. et al. Applications of single-cell RNA sequencing in spermatogenesis and molecular evolution. *Zool Res.* **45**, 575–585 (2024).
70. Yang D. et al. UCHL1 regulates adiponectin receptors in Sertoli cells to maintain testicular homeostatic balance. *J. Biol. Chem.* **301**, 110221 (2025).
71. Wei, Y. et al. Primordial germ cell-like cells derived from canine adipose mesenchymal stem cells. *Cell Prolif.* **49**, 503–511 (2016).
72. Wu, X. et al. Rapid conversion of porcine pluripotent stem cells into macrophages with chemically defined conditions. *J. Biol. Chem.* **300**, 105556 (2024).
73. Zhang, M. F. et al. Transcription factor Dmrt1 triggers the SPRY1-NF- κ B pathway to maintain testicular immune homeostasis and male fertility. *Zool. Res.* **44**, 505–521 (2023).
74. Li, B. et al. Melatonin promotes the therapeutic effect of mesenchymal stem cells on Type 2 Diabetes Mellitus by regulating TGF- β pathway. *Front Cell Dev. Biol.* **9**, 722365 (2021).
75. Deng, X. et al. Chronic liver injury induces conversion of biliary epithelial cells into hepatocytes. *Cell Stem Cell* **23**, 114–122.e113 (2018).
76. Zhang, Y. et al. O-GlcNAcylation of MITF regulates its activity and CDK4/6 inhibitor resistance in breast cancer. *Nat. Commun.* **15**, 5597 (2024).
77. Zhang, J. et al. Super-enhancers conserved within placental mammals maintain stem cell pluripotency. *Proc. Natl Acad. Sci. USA* **119**, e2204716119 (2022).
78. Love, M. I., Huber, W. & Anders, S. Moderated estimation of fold change and dispersion for RNA-seq data with DESeq2. *Genome Biol.* **15**, 550 (2014).

Acknowledgements

We thank all dog participants for their cooperation. We are grateful to Tingting He and Jialong Wang for their efforts in sample collection and veterinarians Jianwu Mo for taking care of the dogs. We thank Dr. Ejaz Ali Khan for his assistance in writing this article. Special thanks to Longgen Sun for his assistance with the experiment. We are grateful to Ms. Zhenzhen Ma and Mr. Jianchu Zhu (Crop Biology Innovation Center, College of Agriculture, Northwest A&F University, Yangling, China) for their assistance in flow cytometry and laser confocal microscopy experiments. This study was funded by the National Basic Research Program of China (2023YFF1000904, 2022YFD1302200). This work was supported by the National Natural Science Foundation of China (32072806, 32372970; 62472360;62072377), Program of Shaanxi Province Science and Technology Innovation Team (2019TD-036), the Key Technologies Demonstration of Animal Husbandry in Shaanxi Province (20221086, 20230978), and Science Fund for Distinguished Young Scholars of Shaanxi Province (2024JC-JCQN-29).

Author contributions

B.L.L., Y.H.Z. and J.L.H. conceived and designed the study. M.H., Z.Y.Z., ZXL, and W.L.Z. worked on the experiments. H.D. and M.Z.L. analyzed the data. B.L.L., Y.H.D., and J.L.H. drafted the manuscript. B.L.L. and M.H. cultured mesenchymal stem cells (MSCs) and constructed MNAT1-MSCs. The rest

of the authors helped to recruit dogs and collect samples. All the authors have read and approved the final manuscript.

Competing interests

The authors declare no competing interests.

Additional information

Supplementary information The online version contains supplementary material available at <https://doi.org/10.1038/s42003-025-08333-z>.

Correspondence and requests for materials should be addressed to Mingzhi Liao or Jinlian Hua.

Peer review information *Communications Biology* thanks the anonymous reviewers for their contribution to the peer review of this work. Primary Handling Editors: Christopher Hine and Aylin Bircan.

Reprints and permissions information is available at <http://www.nature.com/reprints>

Publisher's note Springer Nature remains neutral with regard to jurisdictional claims in published maps and institutional affiliations.

Open Access This article is licensed under a Creative Commons Attribution-NonCommercial-NoDerivatives 4.0 International License, which permits any non-commercial use, sharing, distribution and reproduction in any medium or format, as long as you give appropriate credit to the original author(s) and the source, provide a link to the Creative Commons licence, and indicate if you modified the licensed material. You do not have permission under this licence to share adapted material derived from this article or parts of it. The images or other third party material in this article are included in the article's Creative Commons licence, unless indicated otherwise in a credit line to the material. If material is not included in the article's Creative Commons licence and your intended use is not permitted by statutory regulation or exceeds the permitted use, you will need to obtain permission directly from the copyright holder. To view a copy of this licence, visit <http://creativecommons.org/licenses/by-nc-nd/4.0/>.

© The Author(s) 2025